JOINT INSTITUTE FOR AERONAUTICS AND ACOUSTICS

National Aeronautics and
Space Administration
Ames Research Center

JIAA TR - 56

Stanford University

VERIFICATION OF PERFORMANCE RESULTS FOR A LOW-SPEED 15% ELIPTICAL CIRCULATION CONTROL AIRFOIL

BY

L. C. Rodman and N. J. Wood

Stanford University
Department of Aeronautics and Astronautics
Stanford, CA 94305

FEBRUARY 1986

J I A A T R - 5 6

VERIFICATION OF PERFORMANCE RESULTS FOR A LOW-SPEED 15% ELLIPTICAL CIRCULATION CONTROL AIRFOIL

L. C. Rodman, N. J. Wood

February, 1986

The work presented here has been supported by the
NASA Ames Research Center under contract
NAG 2-173 'Circulation Control Aerodynamics'

ABSTRACT

Low-speed wind tunnel tests performed by the Naval Ship Research and Development Center on a circulation control airfoil model have been repeated by the Joint Institute for Aerodynamics and Acoustics at Stanford University in an attempt to reproduce the performance results. The model used was a 15% ellipse with interchangeable trailing edges on loan from NSRDC. Surface pressure measurements were taken to obtain lift and pitching moment coefficients as functions of jet blowing momentum, and the momentum deficit in the wake was measured and used to calculate the drag coefficient. The effects of spanwise slot height variation and of leading edge blowing on performance were also investigated.

Wall blowing at the 85% chord position was employed to reduce three-dimensional effects, and a solid blockage correction was applied to the free-stream velocity.

The performance results showed that of the three slot heights tested, a slot height:chord ratio of .0022 produced the most lift coefficient for a given blowing rate. Lift obtained in the current test ranged from 2 to 35% lower than in the NSRDC test for the same blowing momentum coefficient. However, the two sets of data compared reasonably well given the differences in the respective wind tunnel test section sizes and wall blowing schemes.

The spanwise lift distribution showed less change in lift due to a variation in slot height than expected. The leading edge blowing results demonstrated that although lift initially decreased, a positive lift increment was possible at higher leading edge blowing rates. Two types of leading edge flow field were apparent, and the jet velocity ratio determined when the flow field switched from the jet folding over the top of the leading edge to the jet continuing around the lower surface.

ACKNOWLEDGEMENTS

The support and advice of Mr. E. O. Rogers and Ms. J. Abramson of NSRDC is gratefully acknowledged, including the generous loan of the circulation control model, the subject of this report.

TABLE OF CONTENTS

SYMBOLS

C_D	2-d total drag coefficient
C_{Dp}	2-d pressure drag coefficient
C_L	2-d lift coefficient
$C_{ml/2}$	half-chord pitching moment coefficient
C_p	pressure coefficient
$C\mu$	coefficient of jet momentum
h/c	slot height:chord ratio
LEC_L	leading edge lift coefficient (lift over the forward half of the airfoil)
$\dot{m}$	mass flow of jet
P	free-stream static pressure
P_d	duct (plenum) pressure
q	free-stream dynamic pressure
R	gas constant
S	model planform area
T	free-stream temperature
V_j	jet velocity
V_∞	free-stream velocity
α	incidence angle
ΔC_L	increase in C_L due to blowing
ΔC_p	difference in C_p between bottom and top of airfoil
γ	ratio of specific heats
ρ_j	jet density
ρ_∞	free-stream density

LIST OF FIGURES

I. INTRODUCTION

Various forms of blowing have been used to augment and control the lift on airfoils independently of incidence. These include such devices as the jet flap and the augmenter wing. Circulation control airfoils employ blowing over a rounded trailing edge to control the lift. Since the trailing edge is not sharp, the usual Kutta condition cannot be enforced and the rear stagnation point is free to move dependent upon the circulation, incidence angle, and free-stream velocity. A two-dimensional spanwise jet of air exits tangentially over the trailing edge, a strong attachment of the jet to the curved surface occurs, and a strong entrainment of the surrounding fluid is evident. This is known as the Coanda effect. The flow remains attached to the curved surface, delaying separation, and thus allows the circulation to be controlled as a function of jet blowing. Since the freedom of the rear stagnation point to move around the trailing edge characterizes an inviscid fluid, a potential flow solution can be shown to approximately model the flow around the airfoil. The large increase in circulation for a small movement of the rear stagnation point allows higher lift augmentations for circulation control airfoils than for other blown airfoil configurations, such as the jet flap and upper surface blowing, typically by a factor of five.

Circulation control, because of its high lift capabilities at low speeds, has many applications in the design of helicopters and V/STOL aircraft. Blowing can be used to control the lift on a helicopter rotor and thus replace mechanical collective and cyclic pitch control. A variation of the slot height along the span of a rotor may be used to contour the load distribution for optimization of blowing requirements and to reduce induced drag effects. Leading edge blowing, where a jet of air is blown tangentially over the leading edge, may be used to increase the lift on a helicopter rotor blade when it is operating in the reversed flow region on the retreating blade side at high advance ratios. The blowing is in the opposite direction of the free stream during most of the rotor cycle, but in the reversed flow region it acts as trailing edge blowing and produces positive lift compared to the usual retreat-

ing blade stall. This reduction of retreating blade stall and corresponding improvement in rotor disc efficiency would enable helicopters to fly at higher advance ratios. For V/STOL applications, circulation control is capable of providing a transition between low-speed helicopter flight and high-speed fixed wing aircraft flight, such as with the X-wing stopped rotor vehicle.

The majority of low speed wind tunnel tests have been performed at the David W. Taylor Naval Ship Research and Development Center (NSRDC). Investigation of the effects of airfoil and trailing edge geometry, slot height, thickness:chord ratio, and camber have been performed. The data taken included lift coefficient, drag coefficient, and pitching moment coefficient for increasing blowing momentum. This test data is necessary for the understanding of the flow phenomena involved in performance trends, and the eventual design of a full-scale three-dimensional rotor. Since wind tunnel testing of blown airfoils is difficult due to the complexity of the testing environment, it was of interest to be able to reproduce the existing performance data on a low speed circulation control airfoil and also to examine the effects of a spanwise slot height distribution and leading edge blowing on performance.

The model to be tested was loaned by NSRDC to the Joint Institute for Aerodynamics and Acoustics (JIAA) at Stanford University. The model had an 8 inch chord and a 15 inch span. The section, which was a 15% thick ellipse with 1% circular arc camber (figure 1), had previously been tested at NSRDC, with the results given in reference 1. The Stanford tests subsequently took place during the spring and fall of 1982. The model was placed in the Stanford low speed 18" x 18" wind tunnel, and performance data was obtained using a Scanivalve pressure measuring system. Two trailing edge geometries and three slot height:chord ratios were tested over a range of incidence angles and blowing momentum coefficients. To investigate spanwise lift distribution, the slot height was varied along the span and the performance tests were repeated. The model chord was turned through 180 degrees in the tunnel to investigate leading edge blowing.

II. RESULTS OF PREVIOUS WORK

Reference 1 describes the performance results obtained for the cambered elliptic circulation control airfoil section when tested in a low speed 15" x 20" wind tunnel at NSRDC. The model had two interchangeable trailing edges, one a circular arc and the other a spiral, enabling a comparison of two different geometries. The model was equipped with an internal plenum chamber and a spanwise rectangular slot on the upper surface near the trailing edge. The slot height could be adjusted to any desired value, to a maximum of 0.040 inches.

Two-dimensional tests were performed, and lift and pitching moment coefficients were obtained from pressure tap readings about the center span of the model. Two corrections were applied to the measured quantities: jet reaction components were included in the lift and moment coefficients, and a solid blockage correction was applied to the free-stream dynamic pressure. No wake blockage factor was applied.

Wall blowing was used to ensure two-dimensional flow. Blowing was provided both at the leading edge and at the 70% chord position, and the two positions were regulated independently of each other. To maximize effectiveness, the wall blowing was varied with the model internal duct pressure.

The jet momentum coefficient, $C\mu$, was determined by measuring the jet mass flow using a calibrated orifice plate, and by calculating the jet velocity assuming an isentropic expansion from the plenum. The momentum coefficient was defined as

$$C\mu = \frac{\dot{m} V_j}{q S} . \qquad (1)$$

At a free stream dynamic pressure of $q = 957.60\ N/m^2$, $C\mu$ was varied from 0 to .24. The incidences tested ranged from -20^o to $+10^o$, and tests were run with slot height:chord ratios varying from .0015 to .003. The slot height expanded as the duct pressure was increased, and account was taken of the variation.

For both trailing edge configurations, the lift and drag characteristics at lower blowing rates are similar. A maximum C_L of 4.75 at h/c=.0015 was reached at $\alpha = -4^o$ and $C\mu = .227$ for the circular arc trailing edge. For the

spiral, the test range was limited by tunnel floor interference, but a maximum C_L of 4.53 was obtained at that slot height with $C\mu$ =.180 and -2° incidence.

The maximum lift augmentation ($\Delta C_L/C\mu$) obtained was approximately 60 for each trailing edge. Lift augmentation in these tests was defined as the increase in lift coefficient from the unblown to the blown value for a given $C\mu$. In more recent reports on circulation control performance, the lift augmentation is defined differently as $\partial C_L/\partial C\mu$, the local slope of the lift curve; however, in this report, lift augmentation was defined as $\Delta C_L/C\mu$, in order to be consistent with reference 1.

The effect of slot height on lift performance was shown to be dependent on the incidence and the momentum coefficient. For values of $C\mu$ below .08, higher lift augmentations were produced at h/c=.0015 than at .0022 for both trailing edge configurations. Above $C\mu$ =.08, this trend reversed, and higher augmentations occurred at h/c=.0022. At h/c=.003, the lift augmentation was lower than that produced at the other two slot heights.

III. EXPERIMENTAL PROCEDURE

A. Facilities and Equipment

The same model used in the NSRDC report was used in the present investigation. The model was tested in the 18" x 18" Stanford Subsonic Wind Tunnel. The wind tunnel had a maximum dynamic pressure of 2030 N/m^2, and turbulence levels of less than 0.5%. Variations in dynamic pressure are less than 2% across the section. Since the model had only a 15" span, endplates were fitted and the model was mounted symmetrically about the centerline of the test section, leaving a 1 1/2 inch space between endplate and wall. It was necessary to use wall blowing on the endplates to prevent separation of the wall boundary layer and subsequent three-dimensional interference in the tunnel (see section V.A.). The endplates were equipped with chordwise wall blowing at approximately the 85% chord position (figure 2). The model was equipped with 55 center span pressure taps which were used to calculate the force coefficients, and several sets of spanwise taps which were used to determine two-dimensionality of the flow. The pressure taps were connected to a scanivalve pressure measuring system and controlled by a PDP 11/23 minicomputer. Thirty samples were averaged for each pressure reading after a time delay of 20 msec. A computer program was used which numerically integrated the pressures for lift, leading edge lift, pressure drag, and half-chord pitching moment coefficients. The duct pressure inside the model plenum was measured using a Statham ±25 psia pressure transducer connected to a digital readout. A pitot-static tube was traversed through the wake at one chord length behind the model. Total and static pressures were sampled with the Scanivalve transducers in .05-inch increments through a four-inch traverse of the wake, and the total drag coefficient was calculated using a technique given in reference 2.

The first series of tests were conducted using the circular-arc trailing edge configuration. For these tests, the free-stream velocity was measured in the tunnel with a pitot-static tube placed in the lower front of the test section; however, the velocity reading was affected by the model presence. For the second series of tests using the spiral trailing edge configuration, the tunnel was recalibrated using static pressure taps in the contraction

section upstream of the test section, where model interference was negligible. To account for some of the tunnel interference effects, corrections were made to the measured value of the velocity (see section III.C.).

Both the model blowing and the wall blowing were connected to a 2800 psig, 104 cubic ft. external air supply, with the supplies independently regulated.

B. Test Procedure

Two separate series of tests were conducted: the first uing the circular-arc trailing edge configuration, and the second using the spiral trailing edge. For each series of tests, basic performance data were taken to determine the characteristics of each airfoil. Both spanwise slot height distribution tests and leading edge blowing tests were conducted during each series, and the results from the first set of tests helped to determine the emphasis of the second test.

The basic performance tests were run with three slot height: chord ratios of h/c = .0015, .0022, and .003. The momentum coefficient, $C\mu$, was calculated based on the slot height:chord ratio and the measured values for the duct pressure, according to the equation

$$C\mu = \frac{\dot{m} V_j}{q S} = 4 \frac{h \gamma R T}{c(\gamma-1)V_\infty^2} \left[(P/Pd)^{\frac{1-\gamma}{\gamma}} - 1\right] \qquad (2)$$

The slot height:chord ratio was corrected for expansion of the slot due to pressurizing the duct by using the plot of h/c vs. Pd given in the NSRDC report[1] (figure 3).

Since the momentum coefficient was determined from a different source in this study compared to the NSRDC investigation, a comparison plot of $C\mu$ vs. duct pressure was drawn (figure 4). The comparison shows very good agreement at h/c=.0022 and .003, and reasonable agreement at h/c=.0015, well within the accuracy of the slot height setting. Slight differences in slot height settings between the two tests would have different effects on the calculated values of momentum coefficient. In the NSRDC test, a difference in the measured slot height would affect the mass flow measurement and thus $C\mu$ directly; however, in the present test a slight difference in the slot height would not change the calculated momentum coefficient, since the duct pressure

would be unaffected.

The effect of wall blowing was investigated. It was found experimentally that although wall blowing was used, the effectiveness of maintaining a two-dimensional flow reduced at higher jet blowing. The wall blowing capability was limited by the maximum delivery of the wall blowing pressure regulator.

The tunnel velocity was kept constant at 40 m/s, and data was taken at 5 incidence angles: -8^{o}, -4^{o}, 0^{o}, $+4^{o}$, and $+8^{o}$. $C\mu$ was varied from 0 to .12, with data being taken in increments of approximately .015. The pressure distribution, C_L, C_{Dp}, and $C_{ml/2}$ were calculated at each point. A solid blockage correction was applied to the free-stream velocity.

During the first series of tests using the circular-arc trailing edge, pressure drag measurements were taken. However, in the second test, a wake traverse system was used, and total C_D measurements were made in addition to the pressure drag.

Investigation showed that the presence of a trip strip produced little change in performance, so it was assumed that the model boundary layer was already turbulent at the test Reynolds number. No trip was used during the performance tests.

C. Velocity Corrections

During the initial testing, it was noticed that Cp's in excess of +1.0 and as high as +1.4 were being produced at the leading edge. This was caused by the actual free-stream velocity being higher than the measured free-stream velocity, with the error due to solid and wake blockage in the test section. The pitot tube was located just upstream and under the model, and since the flow field at that point was affected by the model's high lift coefficients, the pitot tube did not maintain its calibration.

A solid blockage correction to the free-stream velocity was applied, but it accounted for only a part of the velocity difference. Additional tunnel blockage was caused by the wake, but was difficult to determine since it was a function of jet blowing and incidence. No wake blockage correction was made during this test.

The solid blockage correction used was the standard correction for a

two-dimensional elliptic airfoil in a rectangular test section (reference 3). This was the same correction used in the NSRDC report, and it was chosen for purposes of comparison. However, in this case, the flow was complicated by the presence of endplates and wall blowing plenums inside the test section, so the correction underestimated the velocity increase due to solid blockage.

D. Spanwise Lift Distribution Measurement

In this experiment, it was necessary to measure the spanwise lift on the airfoil. However, due to an insufficient number of pressure taps at different spanwise stations, it was impossible to integrate directly to find the lift coefficient anywhere except at the midspan. To evaluate the lift along the span, the difference in Cp between the top and bottom pressure tap at the midchord was measured. For potential flow about an ellipse, this ΔCp can be linearly related to C_L for all values of incidence. For a 15% thick ellipse with 1% camber, it is

$$C_L = 1.375\ \Delta Cp\ -\ .1238\ \alpha \qquad (3)$$

The slot height of the airfoil was varied symmetrically about the midspan, with three spanwise distributions tested. It was expected that the lift should increase with slot height along the span, since $C\mu$ varies linearly with h/c for a constant velocity ratio.

E. Leading Edge Blowing

There are two flow regimes of leading edge blowing (figure 5), and it was attempted to identify both these flow conditions. One, at low $C\mu$, is "fold-back" flow, when the jet folds back over the top of the airfoil, and the other, at high $C\mu$, is when the jet continues onto the lower surface.

Two slot height:chord ratios, .0015 and .003, were tested at $C\mu$'s varying from 0 to .12, with data taken at 0^o and $+/-4^o$ incidence. Initial tests were conducted at a fixed free-stream velocity of 40 m/s, but during the later test the tunnel velocity was varied from 30 m/s to 50 m/s to investigate jet

velocity ratio effects. Pressure distributions were used to determine which flow regime had occurred. The solid blockage correction was applied to the free-stream velocity, but no wall blowing was used.

IV. RESULTS

A. Performance

The results of the first tests involving the circular-arc trailing edge are shown in figures 6-15. Figures 6-8 show the variation of lift coefficient with blowing for the 3 slot height:chord ratios. Lift increased with blowing at all incidences, although at the $+8^{o}$ incidence the lift augmentation dropped off at high values of $C\mu$. Figures 9-11 show lift augmentation ($\Delta C_L/C\mu$) versus blowing, where ΔC_L was defined as the increase in lift coefficient from the unblown to the blown value for a given $C\mu$. The lift augmentation was higher for negative than positive incidence angles at values of $C\mu$ less than 0.05. At higher values of $C\mu$, the augmentation dropped off for all incidence. A slot height:chord ratio of .0022 produced higher lift augmentations at a constant $C\mu$ than either .0015 or .003. Peak lift augmentations were shown at h/c=.0015 and .0022 for a value of $C\mu$ between 0.01 and 0.02. At an h/c=.003, this peak was not observed; however, the NSRDC results at that slot height showed a peak augmentation at a $C\mu$ of 0.03. This suggested that the concentration of data points in the present test was too low to show the narrow peak.

Figures 6-8 also show a comparison of the lift curve results between this test and the NSRDC test for 3 incidences. Except for 0^{o} at h/c=.003, the Stanford data ranges from 2 to 35% lower than the NSRDC data. Peak lift augmentations were also higher in the NSRDC results than in the Stanford results.

Pressure drag data for a slot height of .0022 is presented in Figure 12 and half-chord pitching moment data is shown in figures 13-15. The pressure drag coefficient increased with blowing, and the pitching moment became more negative. Both these effects were due to the trailing edge suction peak. Figure 13 also compares pitching moment results between the Stanford and the NSRDC tests for h/c=.0015. The pitching moment was slightly more negative in this test that shown in reference 1.

Additional tests were made with the spiral trailing edge. It was thought that this trailing edge geometry produced more effective Coanda turning than the circular arc. Figure 16 shows the results for a slot height:chord ratio of

.0022. The Stanford results are compared with the NSRDC data. The same trend appeared as with the previous trailing edge. The current lift coefficients range about 18% lower than the NSRDC results for high blowing rates. The loss of performance seen at the highest blowing rates at 0^{o} incidence coincided with the appearance of three-dimensional effects, which affected the midspan pressure taps. A comparison between the two trailing edge geometries in the present test is shown in figure 17. The lift dropped off with the spiral trailing edge, partially due to a lower trailing edge suction peak.

B. Drag Results

Wake profiles were measured during the second test of the spiral trailing edge, and the total drag coefficient was calculated. The correction term $\dot{m}V_{\infty}/qS$ was subtracted from the measured drag coefficient to account for the additional momentum of the jet. Figure 18 shows typical drag plots for circulation control airfoils. The drag coefficient initially decreased with blowing, and then increased sharply at higher values of $C\mu$. The reason for this can be seen in figure 19, which shows wake profiles at various momentum coefficients. At low blowing the wake was as expected for a bluff trailing edge. Then, as blowing was increased, the added jet momentum overcame the momentum deficit in the wake, and the profile became flat and eventually reversed. As the blowing was further increased and the jet was defected downward, an S-shape profile was generated, showing both the momentum deficit due to the wake and the momentum gain due to the jet.

Figure 18 also compares the drag between the NSRDC and Stanford tests for an h/c=.0022. The results at 0^{o} incidence compare well at low blowing, but the Stanford results show the drag rise occurring earlier at higher blowing.

C. Spanwise Lift Distribution

The lift coefficient results for a spanwise slot height variation are shown in figures 20-21. Tests were run at both 0^{o} and -4^{o} incidence; however, since the results were similar at both incidences, only the 0^{o} results are given here. Figure 20 shows ΔCp plotted against spanwise position for various values of $C\mu$ for the straight slot, and figure 21 is for the varying slot

height case. For the straight slot with blowing and for the varying slot with no blowing, the distribution was not quite flat, indicating that the flow was slightly uneven across the span. After blowing was applied to the varying slot, the spanwise lift distribution increased in value, but did not change shape with slot height as expected.

In order to compare these experimental values to expected results, a calculation was made to predict the ΔCp distribution from the h/c distribution. Using equation 2, $C\mu$ was found for each h/c along the span. Then, using experimental curves of ΔCp vs. $C\mu$ for the straight slot at various h/c, ΔCp was obtained along the span. The results of this calculation are shown in figure 21.

D. Leading Edge Blowing

The initial results for the leading edge blowing test are plotted in figures 22-23. For each run, the lift coefficient decreased or remained constant for increasing $C\mu$ until a sudden sharp dip was reached. This sudden drop in lift preceded the switch from "fold-back" flow to the flow where the jet continued around the leading edge. Figure 24 shows pressure distributions for leading edge blowing. During "fold-back" flow, there was a slight suction peak behind the slot, shown in figure 24(b). The switch-over caused the lift to increase sharply, which is seen in figure 24(d) as a sudden occurance of a large suction peak on the upper leading edge in front of the slot.

V. DISCUSSION

A. Test Conditions and Performance

Although it was attempted to reproduce the same test conditions here as in the NSRDC test, some discrepancies were unavoidable which may account for some of the error between the Stanford and NSRDC results. These include downwash effects and difficulties with velocity calibration.

Wall blowing effects on lift are shown in figure 25. The increase in lift was slight, indicating that possibly too little blowing was used. The effectiveness of wall blowing should be investigated in more detail, and could account for some differences in lift between the two studies.

Although wall blowing helped to ensure two-dimensional flow across the span, a downwash still occurred, which changed the effective incidence from the geometric incidence. The effective incidence was found for each run using a simple scheme based on potential flow theory. Since viscous effects in the flow were negligible over the leading half of the airfoil section, the match between the theoretical and experimental pressure distributions was very good on the leading edge, providing the correct effective incidence was used. This introduced another flow parameter, the leading edge lift coefficient, LEC_L, which was used to compare experimental pressure distributions with theory. As seen by equation 3, the potential flow relation between C_L and half-chord ΔCp was independent of incidence. However, by relating LEC_L and ΔCp, incidence dependence was shown. A theoretical pressure distribution, which was calculated from known values of C_L and α, produced the associated values of the LEC_L and half-chord ΔCp enabling a plot of LEC_L versus ΔCp for various angles of incidence to be drawn (figure 26). The slopes of these are identical, and the y-intercepts vary linearly with incidence. A single equation relating LEC_L, ΔCP, and α was obtained from this plot:

$$LEC_L = .675\ \Delta CP + .0363\alpha\ - .06 \qquad (4)$$

By specifying two of the three parameters: LEC_L, ΔCp, or α, the pressure distribution about an ellipse was uniquely determined. LEC_L and ΔCp were found

for each experimental data point. Substitution of these values into the above equation gave an effective incidence for each point. From this, figures 27-29 were generated.

The effect of geometric incidence on the downwash can be seen in figures 27-29. The slope of the lines changed with geometric incidence, indicating that the downwash is greater at negative incidences than positive incidences. As the incidence becomes more positive, the adverse pressure gradient at the top trailing edge becomes less severe, thus weakening the tip vortex that forms at the endplate. At zero blowing, the effective and geometric incidence did not match, due to blockage effects. Different blockage corrections can change the effective incidence at zero blowing (figure 27).

A comparison was made of pressure distributions at an h/c=.0022 and at 0^{o} incidence between the Stanford and NSRDC results. The difference in lift coefficients between the two tests was shown to be partially caused by a loss of upper surface leading edge suction in the Stanford test (figure 30). By comparing the effective incidences between the two tests at similar conditions, it was seen that the Stanford data produced a slightly more negative effective incidence than the NSRDC data, which could account for the loss of leading edge suction. This indicated that downwash effects were a major cause of the difference between the results.

The Stanford wind tunnel test section height was 2 inches less than the NSRDC tunnel, which made blockage problems more severe. The model chord:tunnel height ratio, .44, was large for a blown airfoil test. This ratio should be kept under 0.3. The free-stream velocity measurements from the pitot tube could have produced some of the difference in lift coefficients because of the proximity of the pitot tube to the model.

To check the effectiveness of the solid blockage correction, experimental leading edge pressure distributions were compared with theoretical distributions for the same leading edge C_L at the deduced effective incidence. This was done for two blowing cases, shown in figures 31-32(a). In the first case, figure 31(a), the experimental Cp's were offset from the theoretical, indicating a possible error in the tunnel dynamic pressure. In the second case, figure 32(a), the offset was still present, although not as large.

Assuming that a proper velocity correction would produce a stagnation Cp of approximately +1.0, this factor was found and multiplied by all the pressures

to produce a new leading edge C_L and effective incidence. These pressures were compared with a new theoretical distribution, with the results shown in figures 31-32(b). In both cases the offset had disappeared, producing a very good match with potential theory. This was only tried with two experimental pressure distributions and was not applied as a correction to the performance results. However, it is possible that an inverse technique may be employed in the future to derive the blockage correction directly from pressure distribution comparisons.

As an additional check, another solid blockage correction was applied to the data for comparison with the first. This was a two-dimensional mass flow correction, where the velocity increase is proportional to the flow area decrease around the model. This correction overestimates the velocity increase due to solid blockage, and provided a good contrast to the original correction. Figure 33 shows the change in the lift curve depending upon the velocity correction.

The comparison between experimental and theoretical pressure distributions was repeated for the two-dimensional mass flow correction, also shown in figures 31-32(c). There was still an offset between the two, although it was slightly reduced from the offset in the original correction. This showed that the increased velocity was closer to the actual velocity, but an additional wake blockage factor was still needed.

The effective incidence was calculated for the second blockage correction and compared with the original (figure 27). It was seen that the slopes of the lines had not changed, but the effective incidence at zero blowing had moved closer to the geometric incidence. This again indicated that the original solid blockage correction underestimated the free-stream velocity increase.

B. Spanwise Slot Height Distribution

For the cases tested, a spanwise slot height distribution did not produce a significant change in lift along the span. Since $C\mu$ varies linearly with h/c, increasing the slot height should increase the local $C\mu$ and thus the local sectional lift coefficient. However, since the performance varies with slot height, an increase in $C\mu$ might not produce as much of a lift increase as expected, due to a degradation of performance at a larger slot height. In

comparison with the spanwise lift produced from a straight slot, the effect of the slot variation was negligible.

Other slot height distributions were tested during the second test, including one where the original distribution was inverted such that the larger slot height was at the ends rather than in the middle of the span. This change also did not produce a significant change in spanwise lift. Since the model had an aspect ratio less than two, and since there were slight three-dimensional effects apparent along the span, the results produced could have been caused by bad test conditions. Further two-dimensional testing of straight slot heights is necessary to gain a better understanding of how the slot height affects performance. Once the relation of slot height to performance is known, it will be more apparent how the slot height could be varied along the span to contour the lift distribution.

C. Leading Edge Blowing

Leading edge blowing tests were performed to investigate the effect of a forward facing blown slot on lift. At low leading edge blowing, the jet could not oppose the free stream because of insufficient momentum, and "fold-back" flow occurred over the model. As the blowing was increased, a sharp drop in the lift curve occurred just prior to the point where the jet began to continue around to the lower surface (figure 22-23). This was caused by a loss of suction over the upper leading edge, and a corresponding increase in suction over the lower leading edge (figure 24). This drop became less severe as the incidence went from positive to negative, and at -4^{o}, had almost vanished. Slot height effects were apparent from the first tests involving the circular-arc leading edge. The change in flow field from "fold-back" flow to where the jet continues around occurred at a higher blowing rate at h/c=.003 than at .0015 (figure 22-23). As the slot height was doubled, the change in flow occurred at approximately twice the value of $C\mu$. This indicated a strong jet velocity ratio dependence, since $C\mu$ can be defined as

$$C\mu = 2 \frac{\rho_j}{\rho_\infty} \frac{h}{c} (V_j/V_\infty)^2 \qquad (5)$$

When plotted against jet velocity ratio, the switch occurred at comparable ratios for both slot heights (figures 34-35). The second series of tests were

planned to show more clearly the effect of velocity ratio on the leading edge flow field. The earlier tests were repeated at three different free-stream velocities: 30, 40, and 50 m/s. The results can be seen in figures 36-37, which show lift coefficient plotted against jet velocity ratio. For all slot heights, incidences and free-stream velocities tested, the switch in flow field occurred at an approximately constant jet velocity of 5. This was constant also for both leading edge geometries. Slight variations can be seen at different free-stream velocities, possibly due to low Reynolds number effects. The corresponding Reynolds numbers based on model chord were 0.42×10^6, 0.56×10^6, and 0.70×10^6 for 30, 40, and 50 m/s respectively.

A hysteresis in the flow switch occurred depending upon increasing or decreasing blowing (figure 38). The switch occurred at a higher velocity ratio when the jet was folded over the top of the leading edge and the blowing was increased. When the jet is continuing around the lower surface and the blowing was decreased, the switch occurred later, at a lower velocity ratio, perhaps showing that the jet was more stable if it was continuing around the lower surface than if it was folded back over the top. The curve in figure 38 showed good repeatability if the flow was increased, decreased, and then increased again. The nature of the hysteresis did not depend upon free-stream velocity.

The leading edge flow field dependent upon the jet velocity ratio would have implications in the design of full-scale dual blown rotors. With a constant jet velocity and a varying effective free-stream velocity along the span, the rotor could experience both flow regimes at different spanwise stations simultaneously. Due to the hysteresis, this would also be dependent upon whether the rotor was advancing or retreating. Further investigation is necessary with a dual blown airfoil to see how trailing edge blowing affects the leading edge flow field.

VI. CONCLUSIONS

Despite some problems in accurately assessing the tunnel dynamic pressure in the Stanford tests, there was good agreement between the Stanford and NSRDC performance data on the low-speed circulation control airfoil. Further investigation into solid and wake blockage effects during testing is necessary for improved correlation.

The spanwise slot height distribution investigated did not produce a large change in spanwise lift distribution. To obtain more conclusive results, further testing should be done with a larger aspect ratio model, and care should be taken that the flow is two-dimensional across the span.

Leading edge blowing can produce positive lift increments at high blowing rates, and its flow field would appear to be primarily dependent upon jet velocity ratio. More study should be done on the combined effects of leading and trailing edge blowing.

The technique of using a potential flow solution to assess the effective incidence was very useful and simple to include, and may yield an improved technique for the assessment of tunnel blockage due to both solid and wake interference.

REFERENCES

1. Abramson, J., "Two-Dimensional Subsonic Wind Tunnel Evaluation of Two Related Cambered 15-Percent-Thick Circulation Control Airfoils," DTNSRDC Report ASED-373, Sept. 1977.

2. Pankhurst, R. C. and D. W. Holder, Wind-Tunnel Technique, Sir Isaac Pitman and Sons, Ltd., London, 1952, pp. 274-283.

3. Pope, A. and J. J. Harper, Low-Speed Wind Tunnel Testing, John Wiley and Sons, Inc., New York, 1966, pp. 307-311.

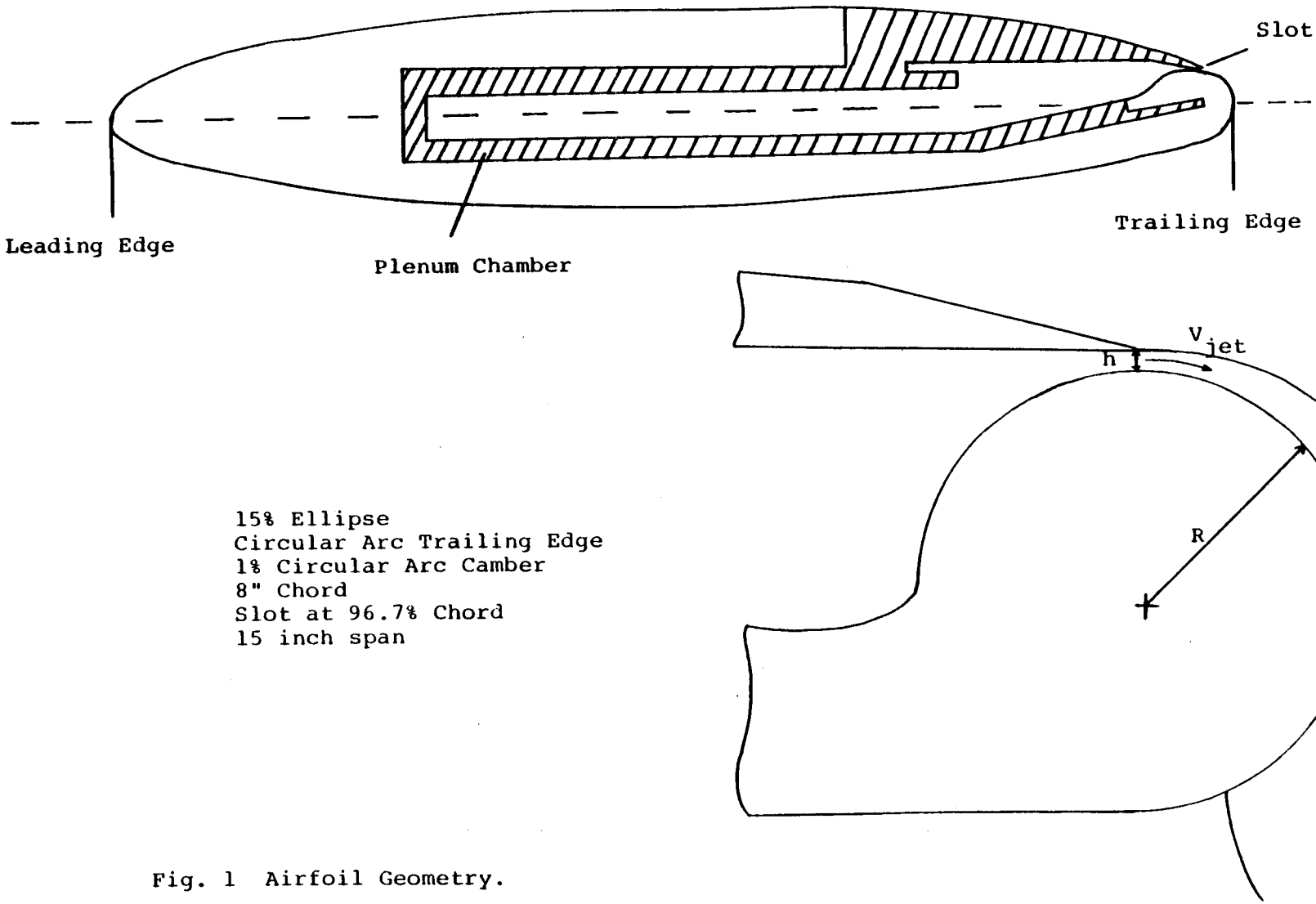

15% Ellipse
Circular Arc Trailing Edge
1% Circular Arc Camber
8" Chord
Slot at 96.7% Chord
15 inch span

Fig. 1 Airfoil Geometry.

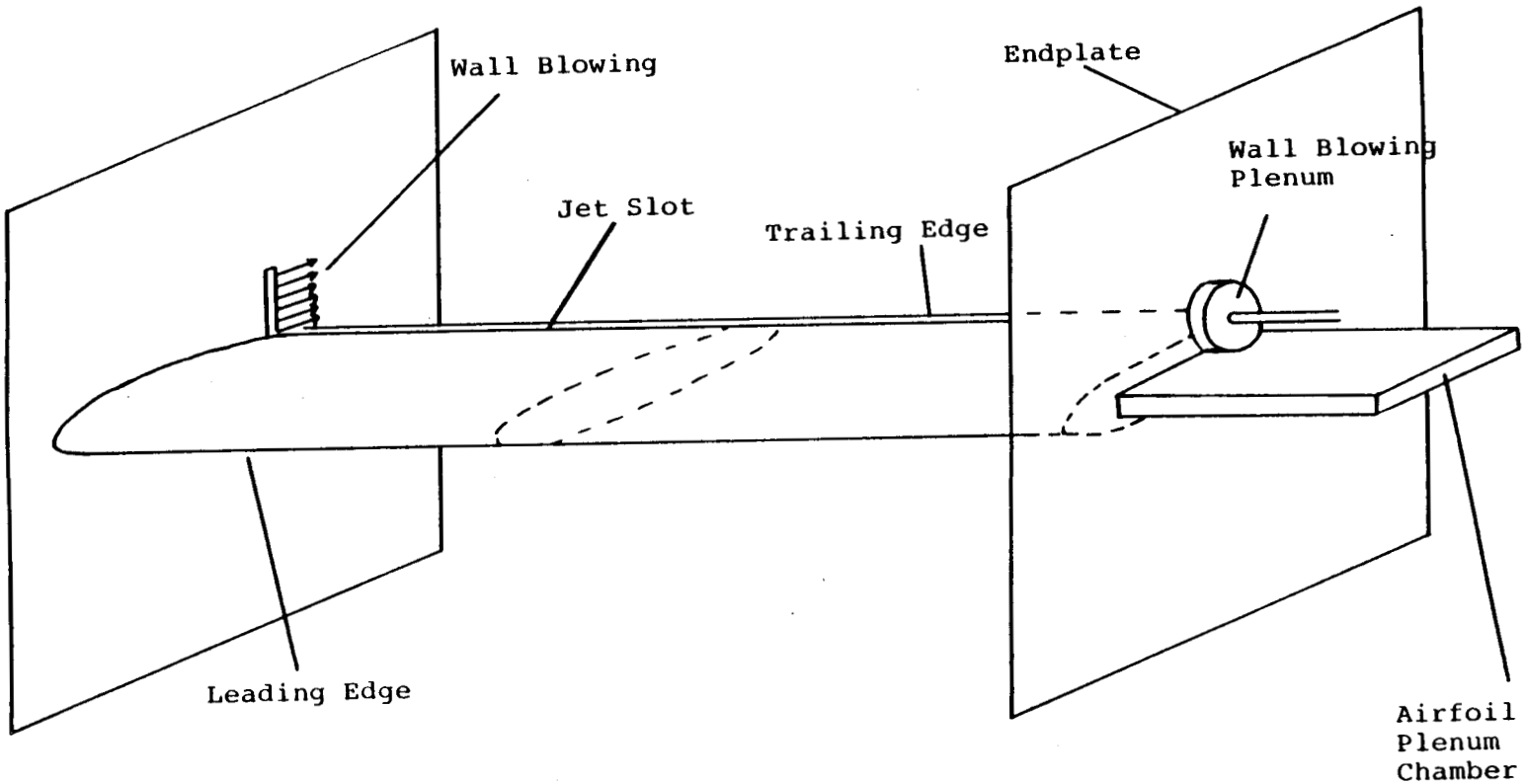

Fig. 2 Airfoil Model with Endplates and Wall Blowing.

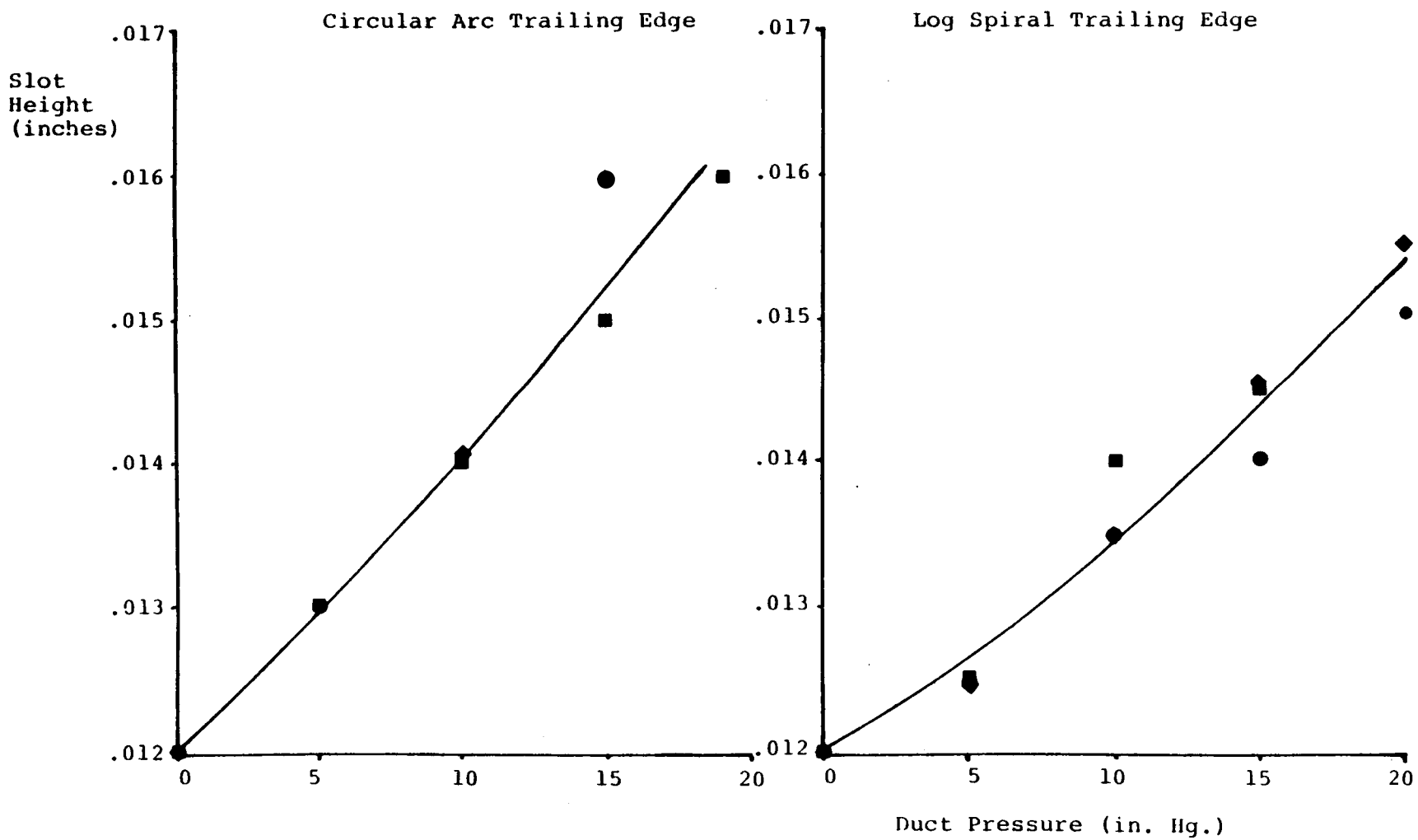

Fig. 3 Variation of Slot Height with Duct Pressure (Ref. 1).

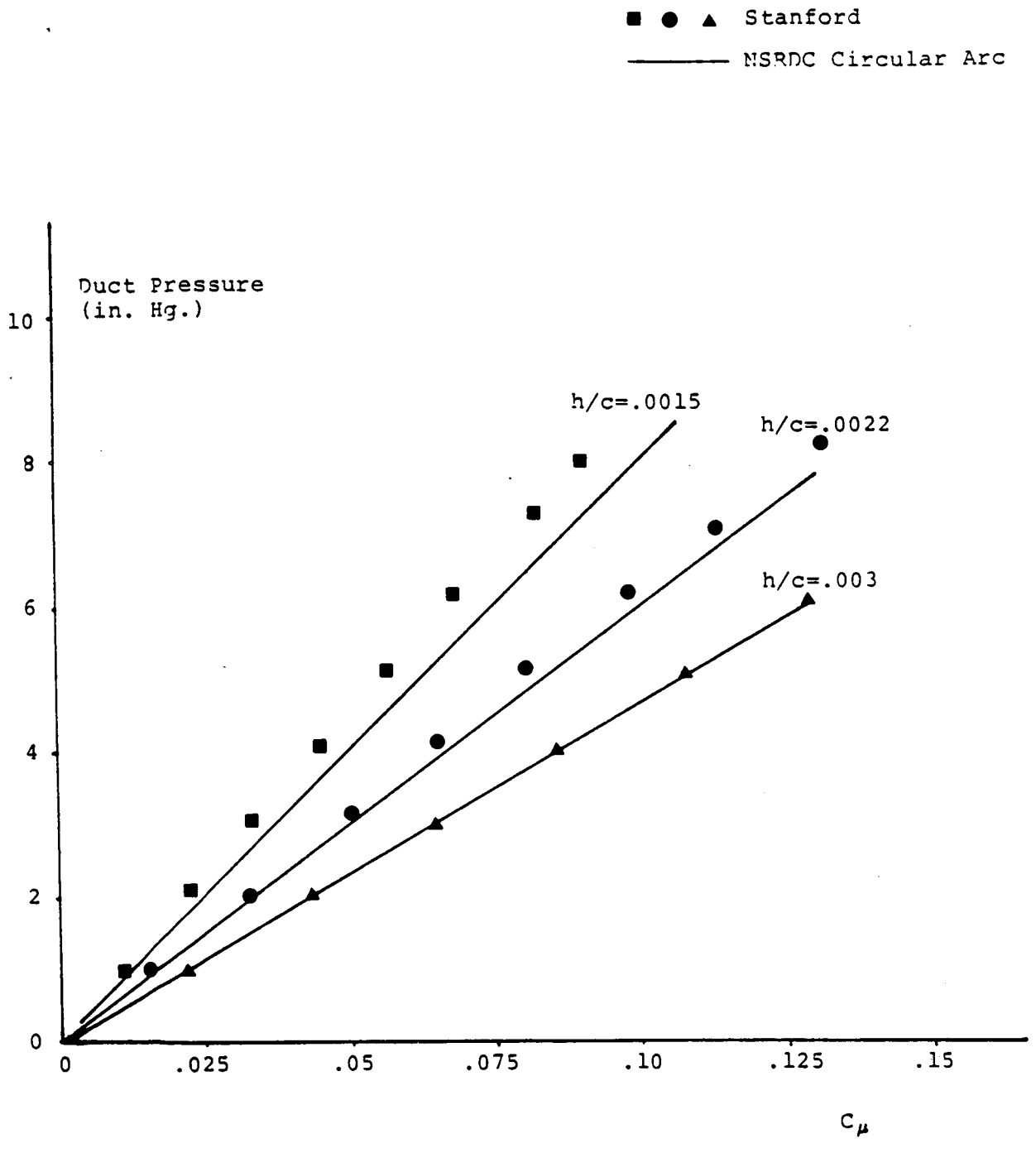

Fig. 4 Duct Pressure vs. Momentum Coefficient: Comparison between NSRDC and Stanford.

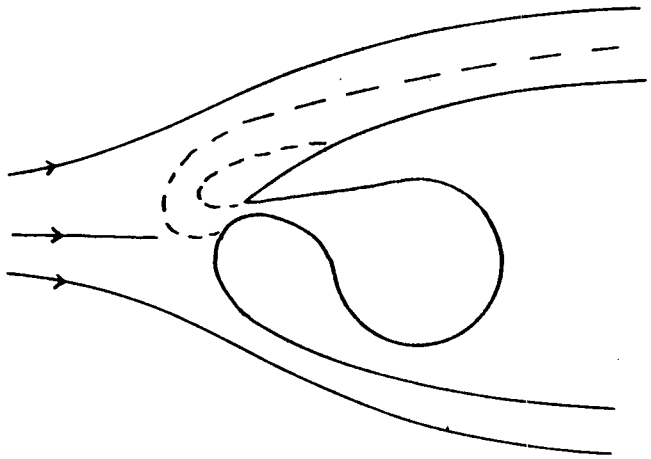

Flow "Folds-Back" at
Lower Blowing Rates.

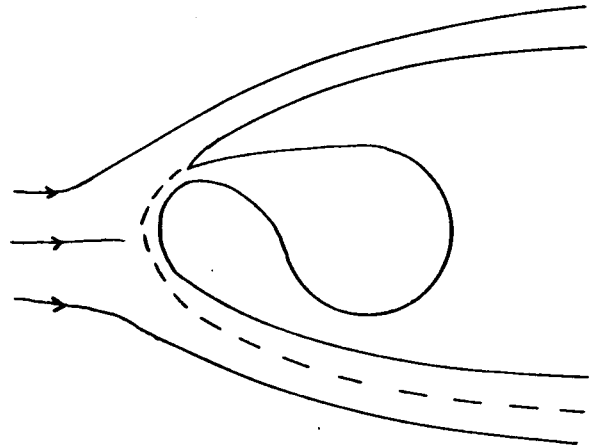

Flow Continues Around Lower
Surface at Higher Blowing Rates.

Fig. 5 Two Flow Regimes of Leading Edge Blowing.

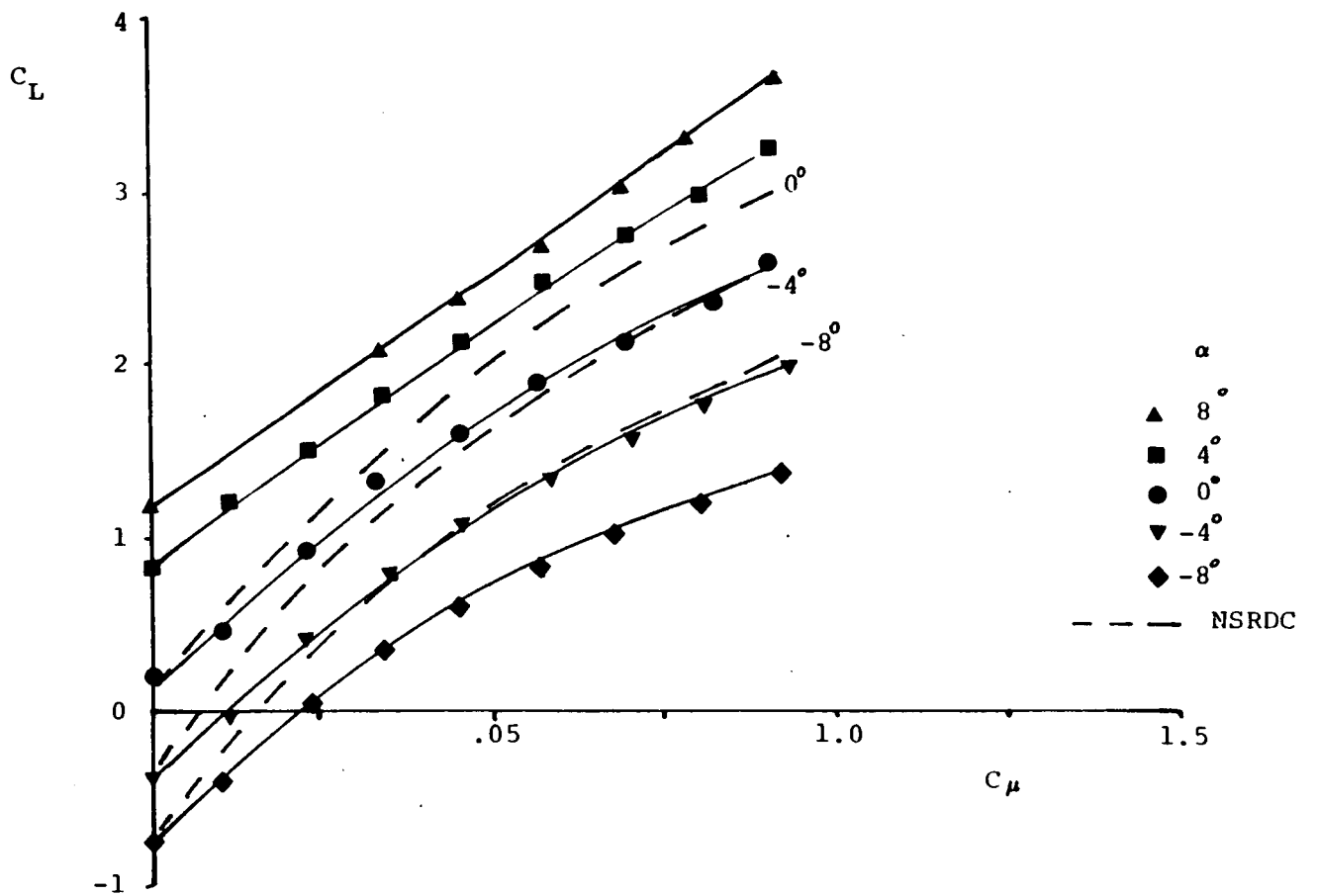

Fig. 6 Lift Coefficient vs. Momentum Coefficient: Comparison between NSRDC and Stanford (h/c = .0015, circular arc trailing edge).

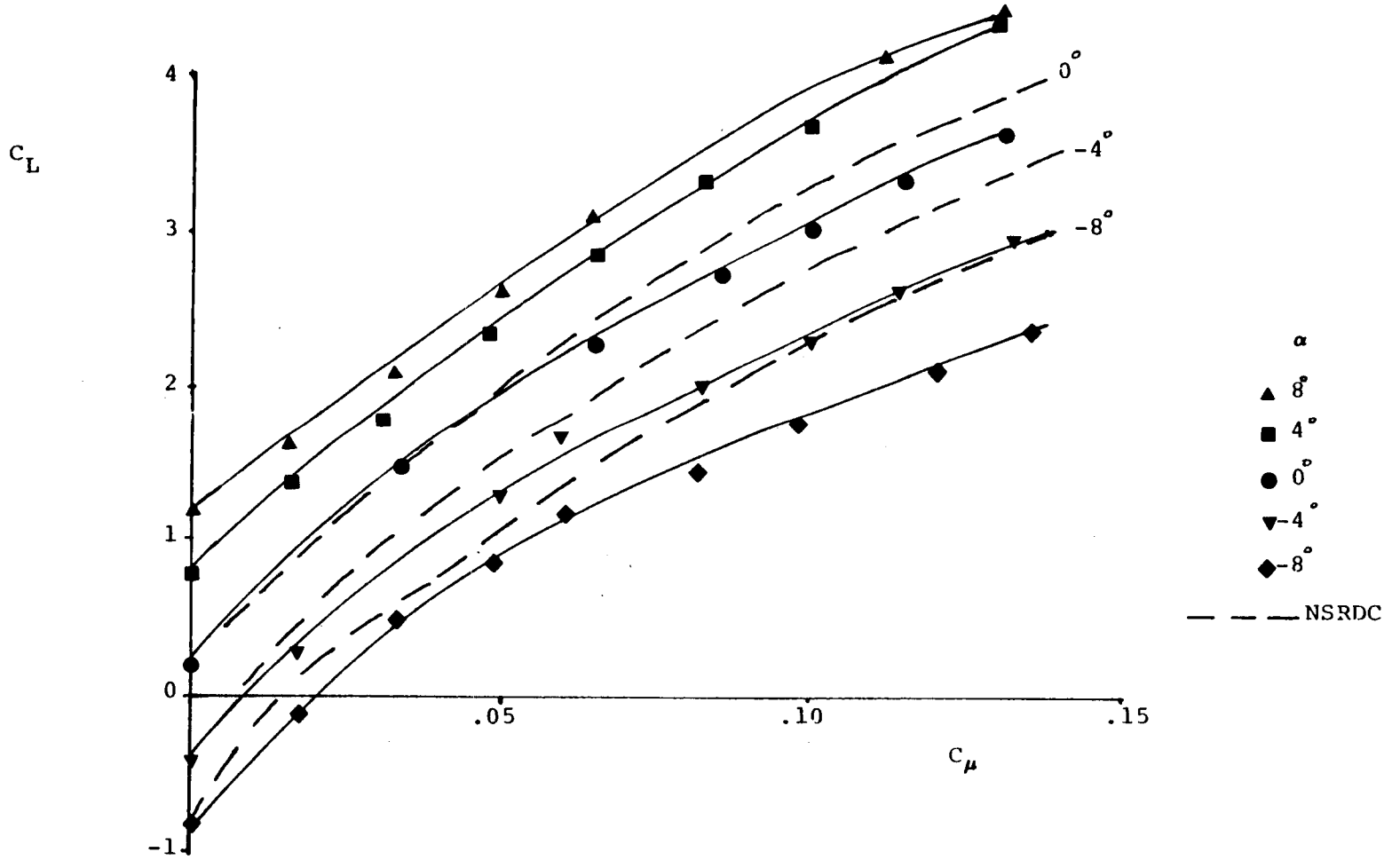

Fig. 7 Lift Coefficient vs. Momentum Coefficient: Comparison between NSRDC and Stanford (h/c = .0022, circular arc trailing edge).

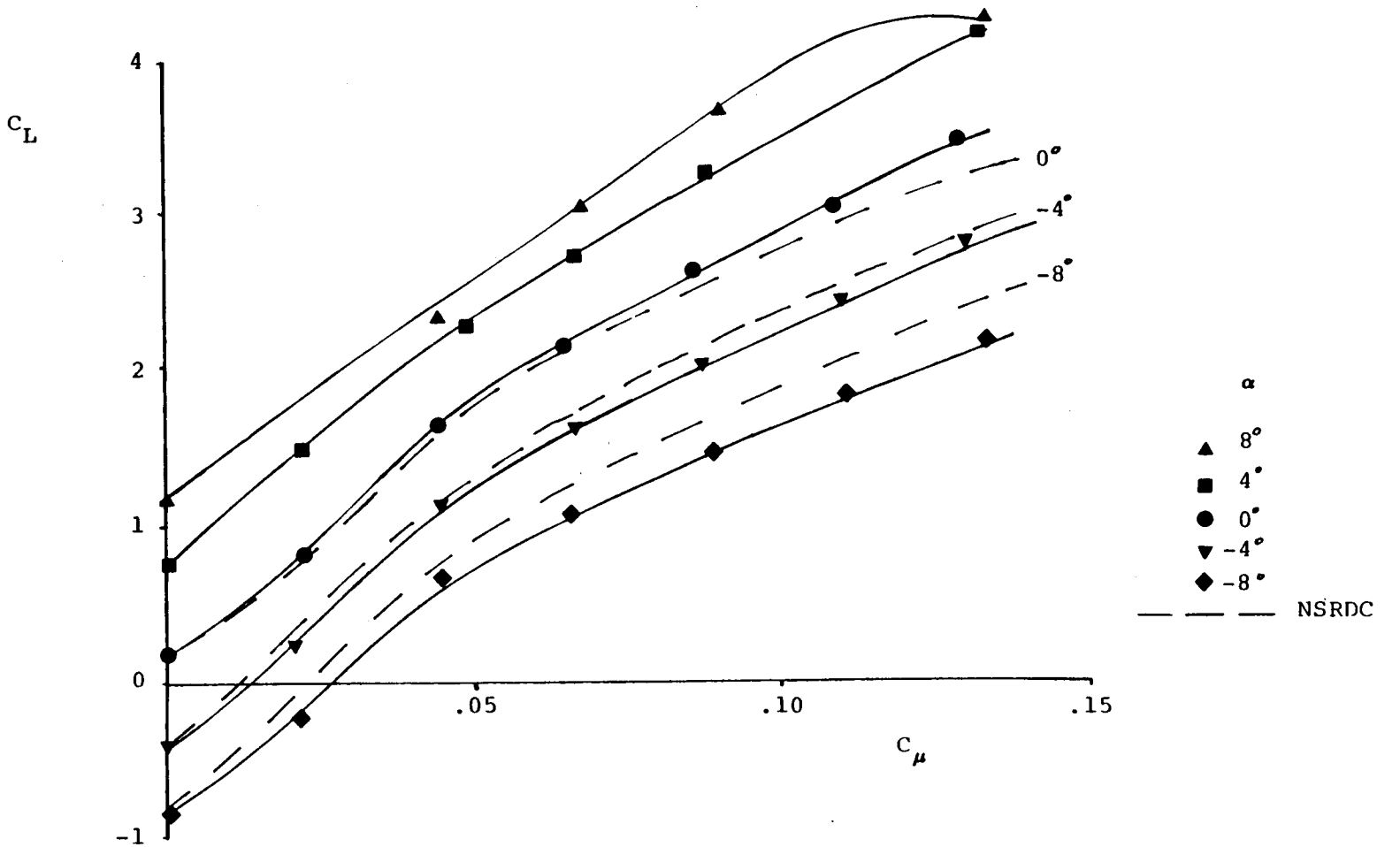

Fig. 8 Lift Coefficient vs. Momentum Coefficient: Comparison between NSRDC and Stanford (h/c = .003, circular arc trailing edge).

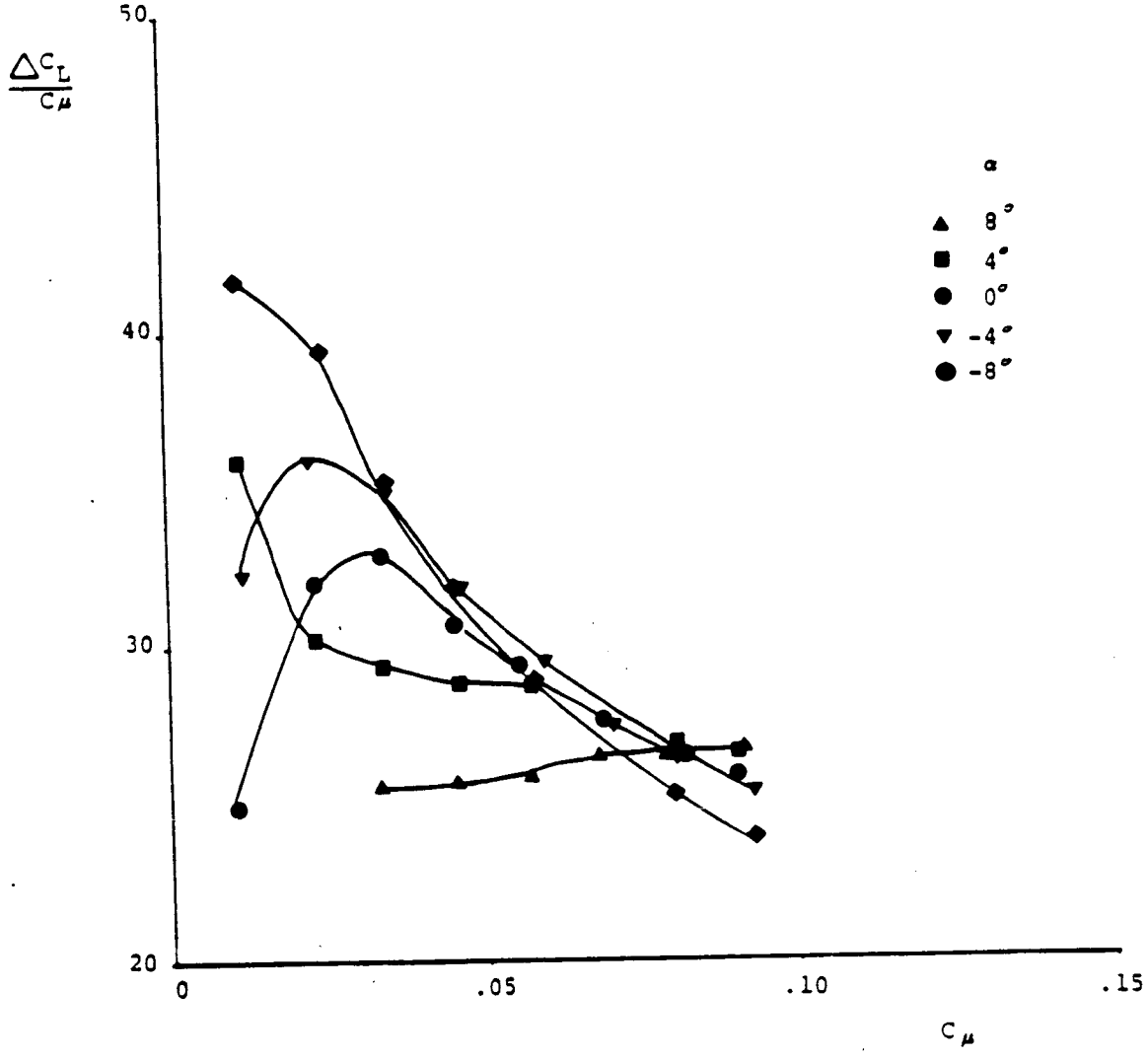

Fig. 9 Lift Augmentation vs. Momentum Coefficient (h/c = .0015).

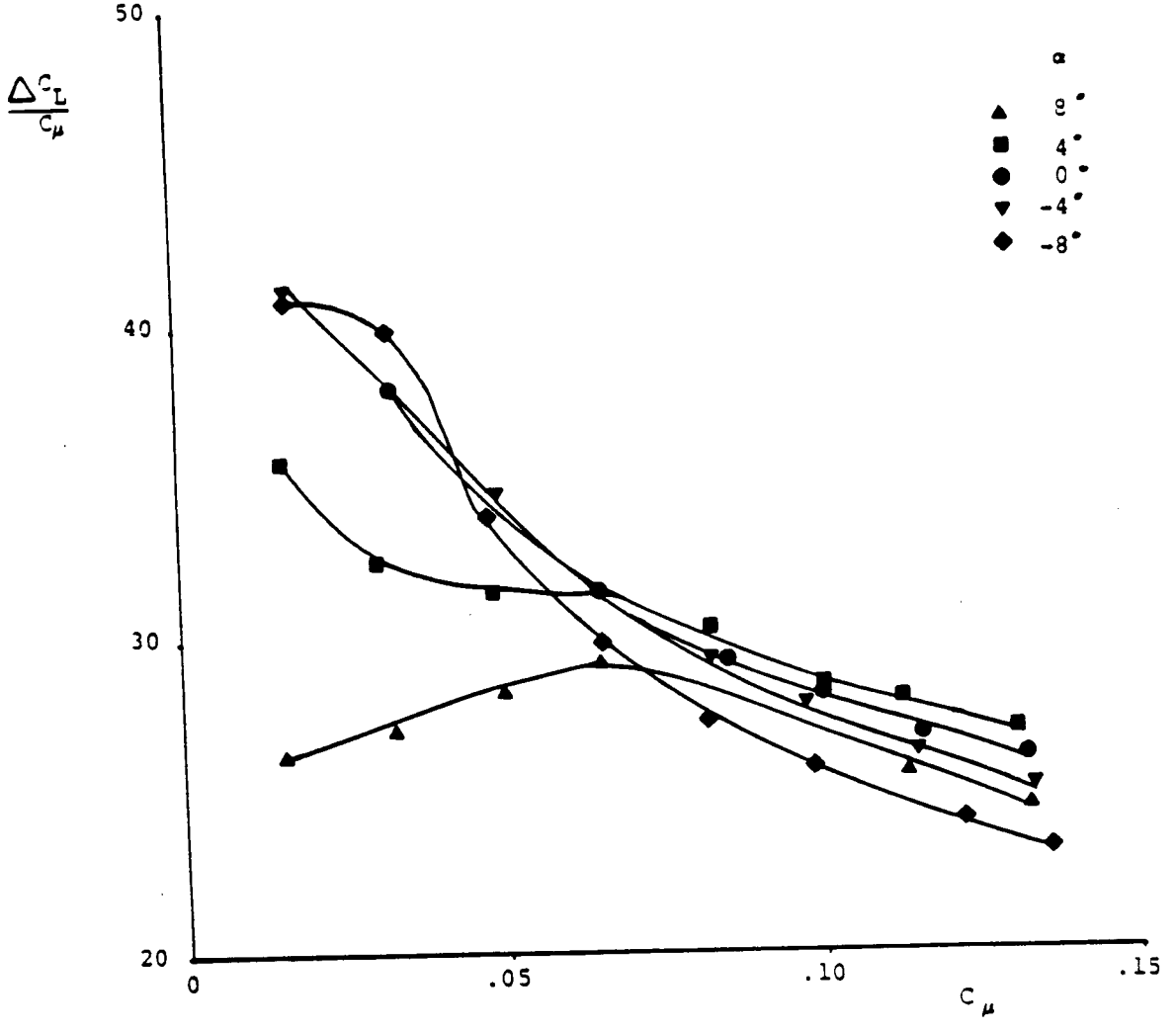

Fig. 10 Lift Augmentation vs. Momentum Coefficient (h/c = .0022).

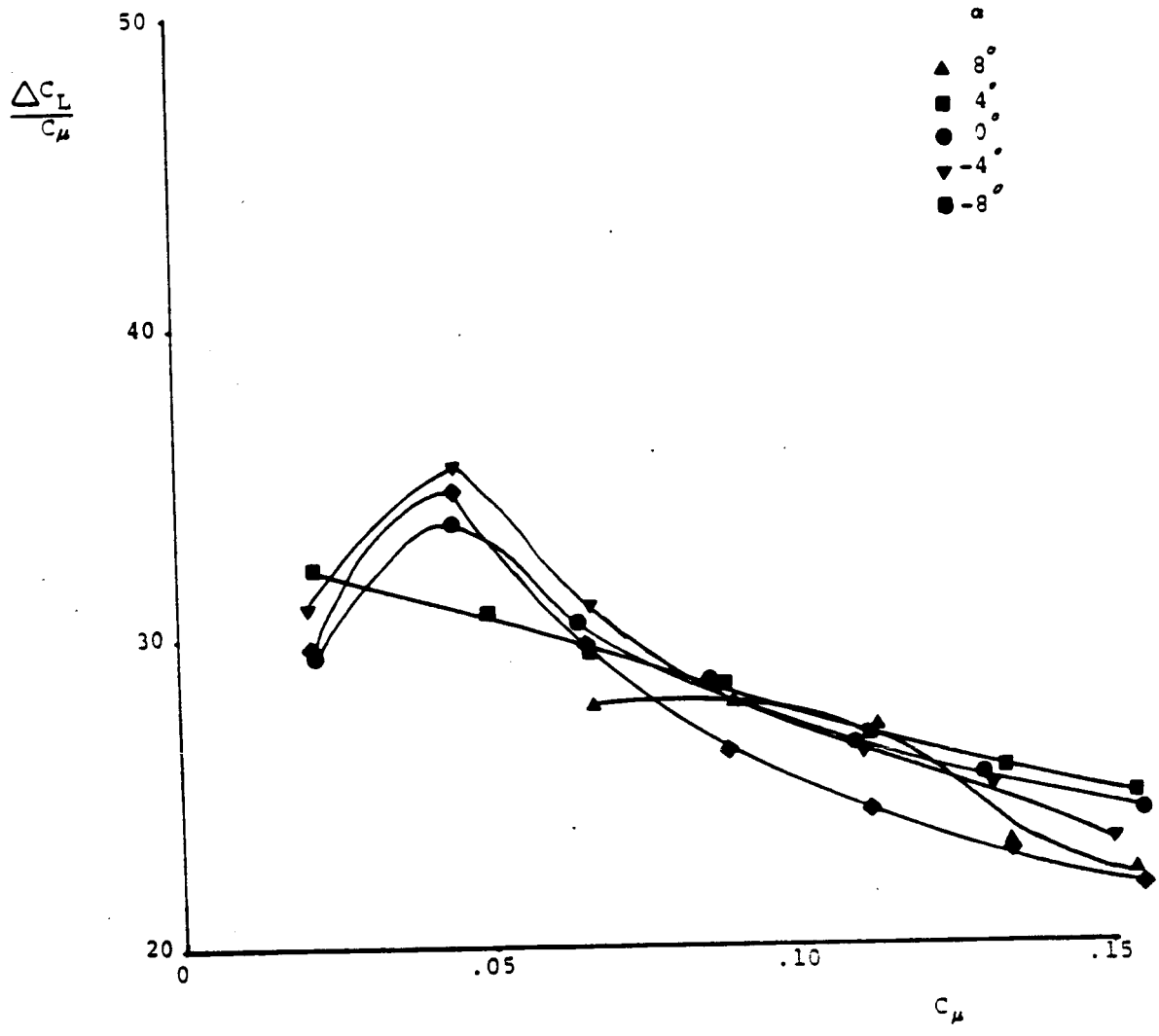

Fig. 11 Lift Augmentation vs. Momentum Coefficient (h/c = .003).

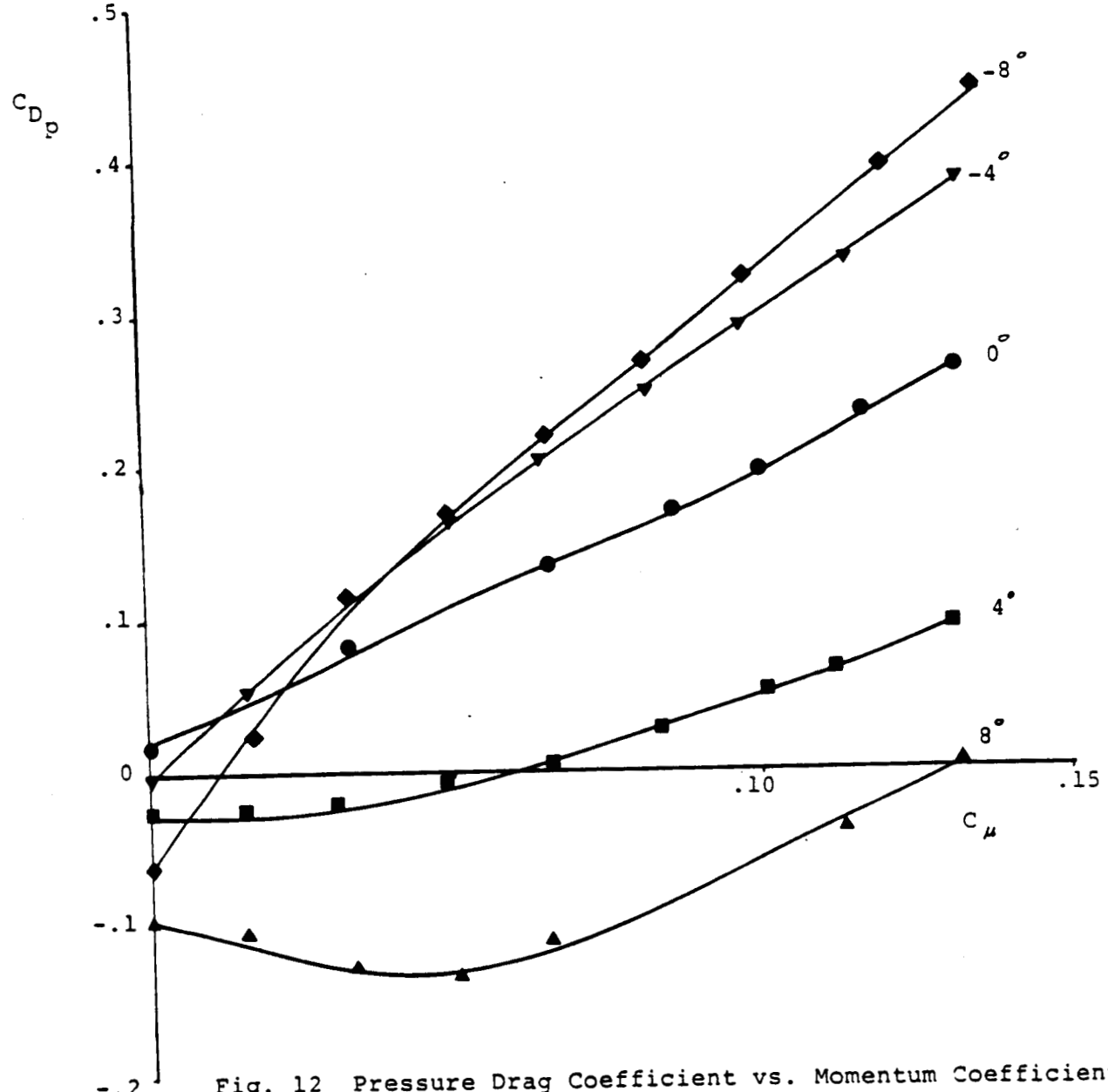

Fig. 12 Pressure Drag Coefficient vs. Momentum Coefficient (h/c = .0022).

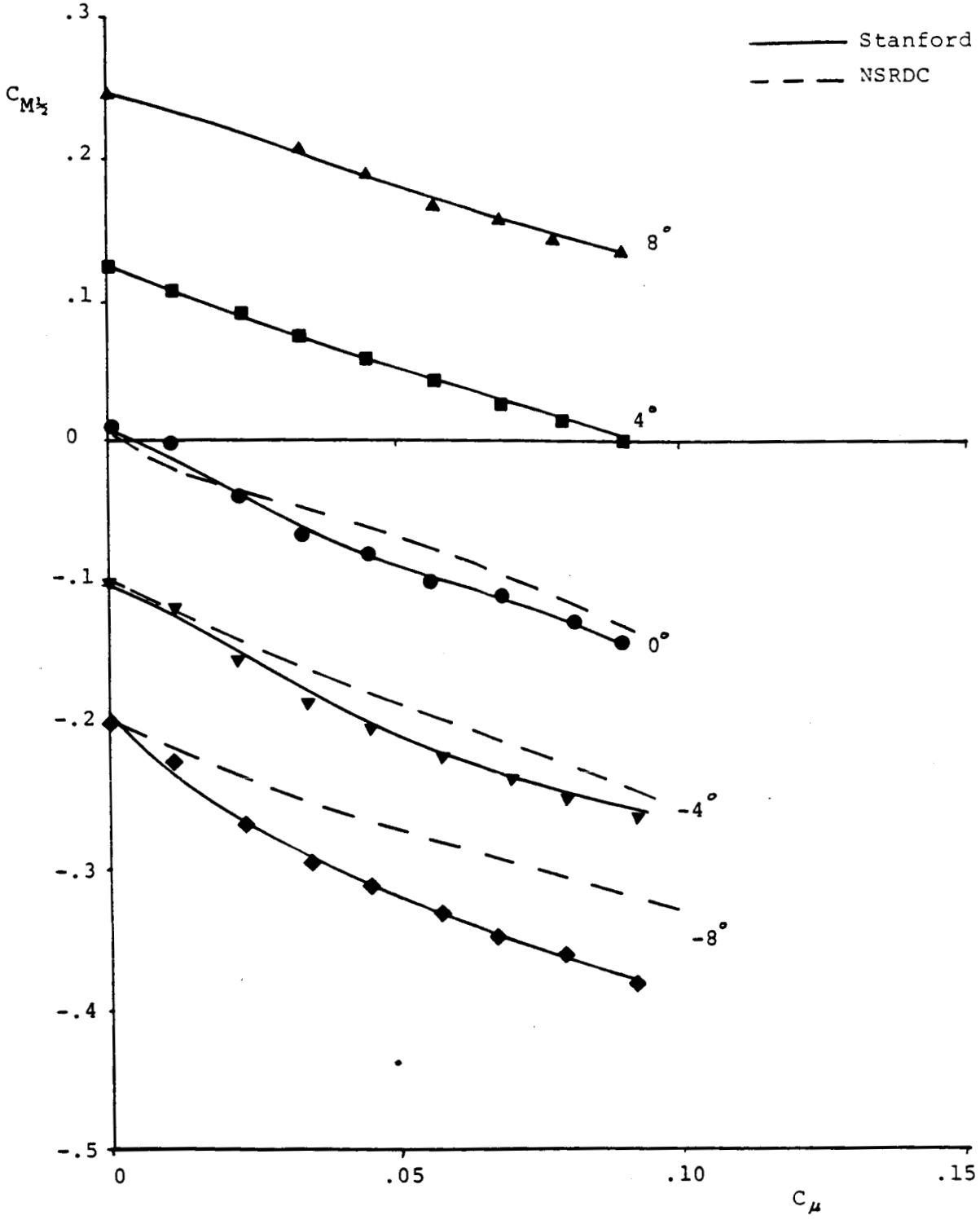

Fig. 13 Half-Chord Pitching Moment vs. Momentum Coefficient: Comparison between NSRDC and Stanford (h/c = .0015).

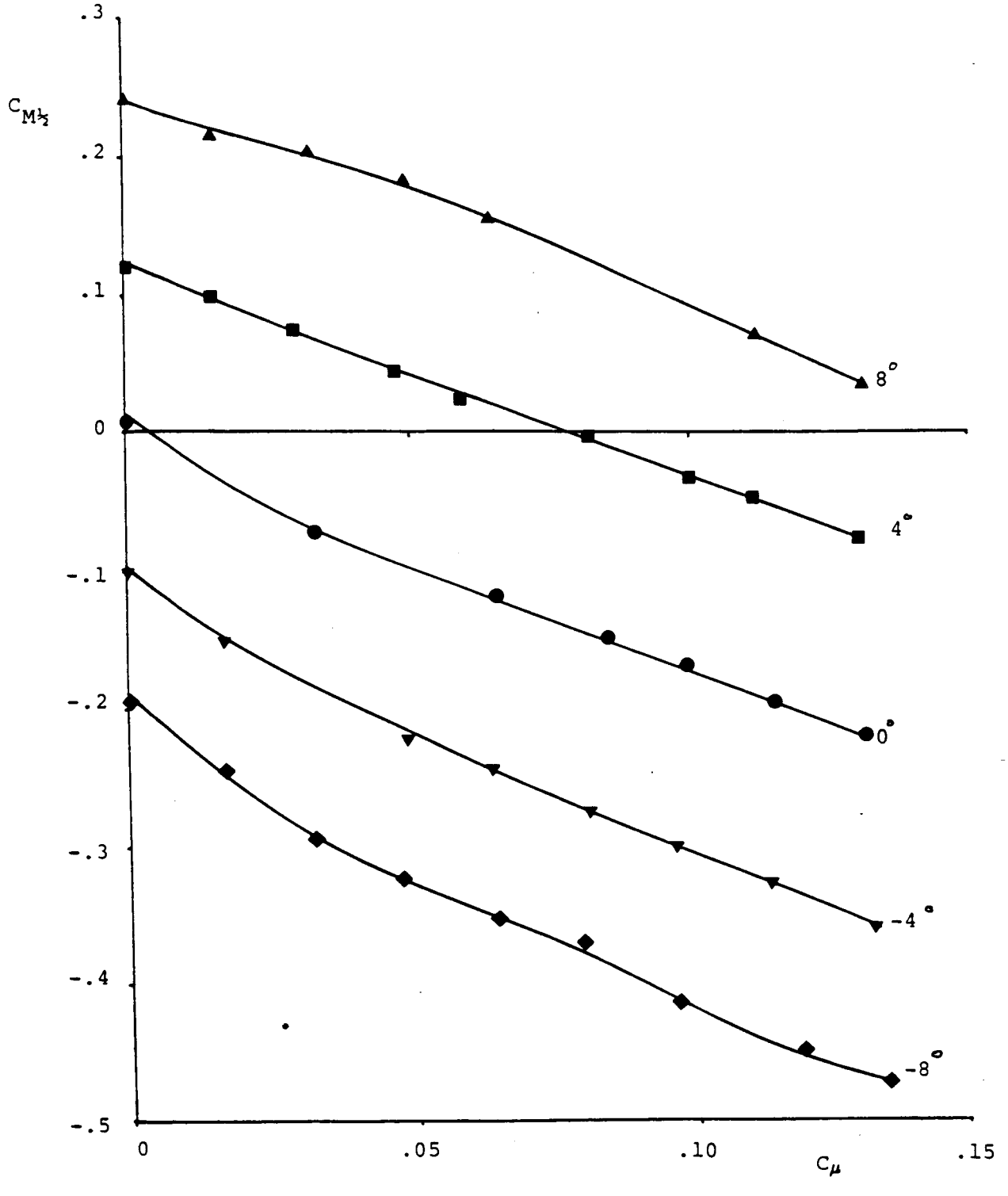

Fig. 14 Half-Chord Pitching Moment vs. Momentum Coefficient (h/c = .0022).

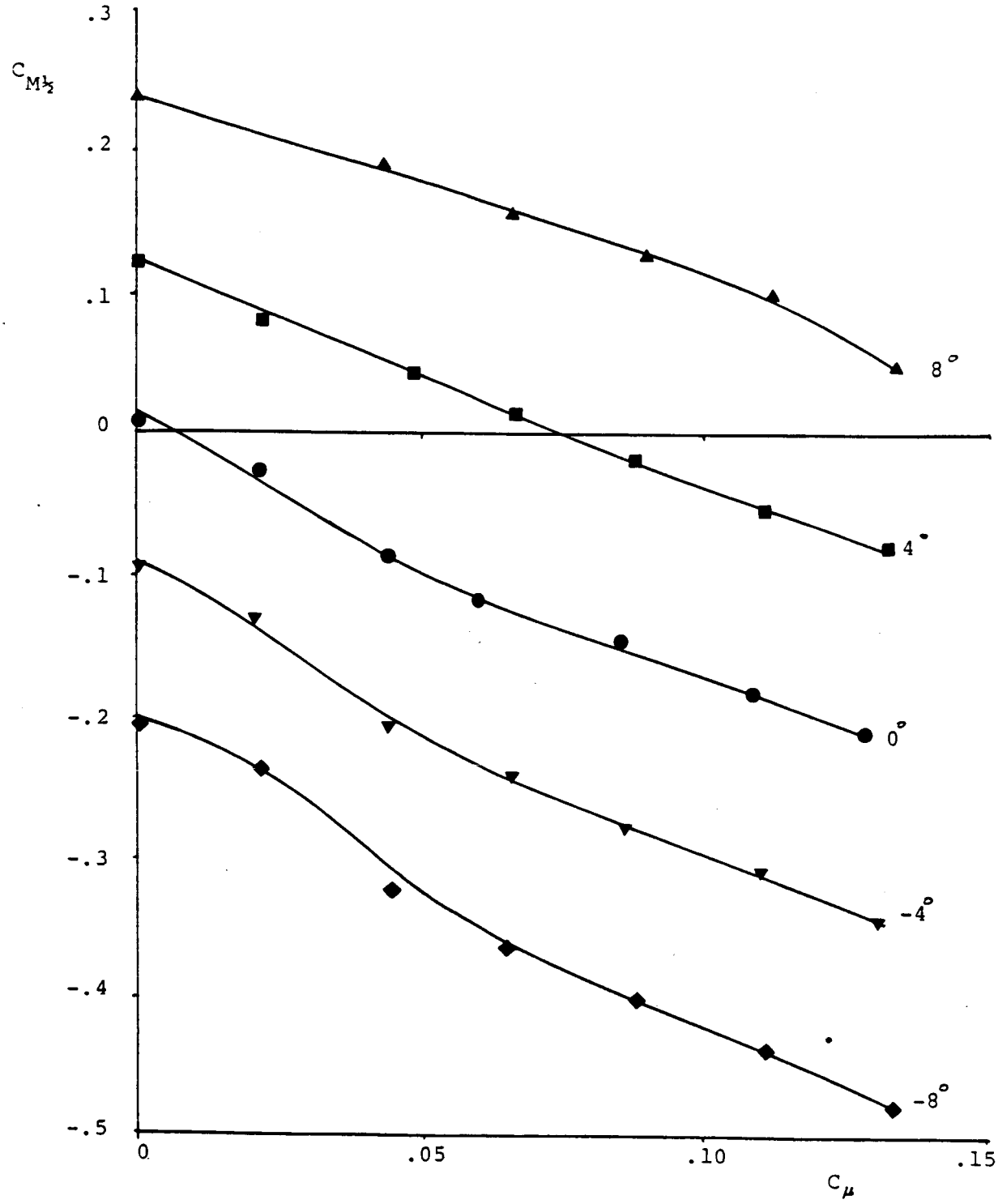

Fig. 15 Half-Chord Pitching Moment vs. Momentum Coefficient (h/c = .003).

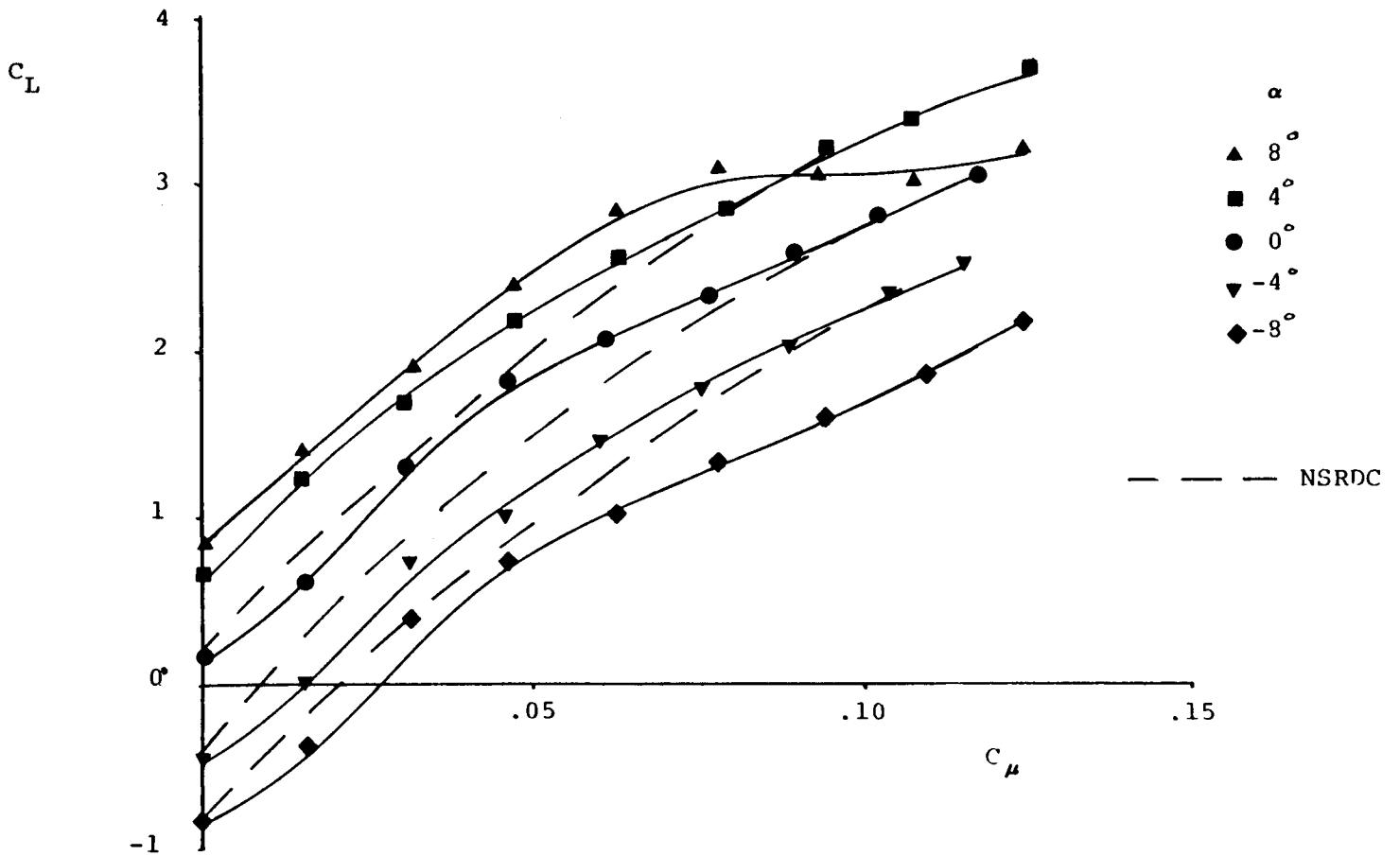

Fig. 16 Lift Coefficient vs. Momentum Coefficient: Comparison between NSRDC and Stanford (h/c=.0022, spiral trailing edge).

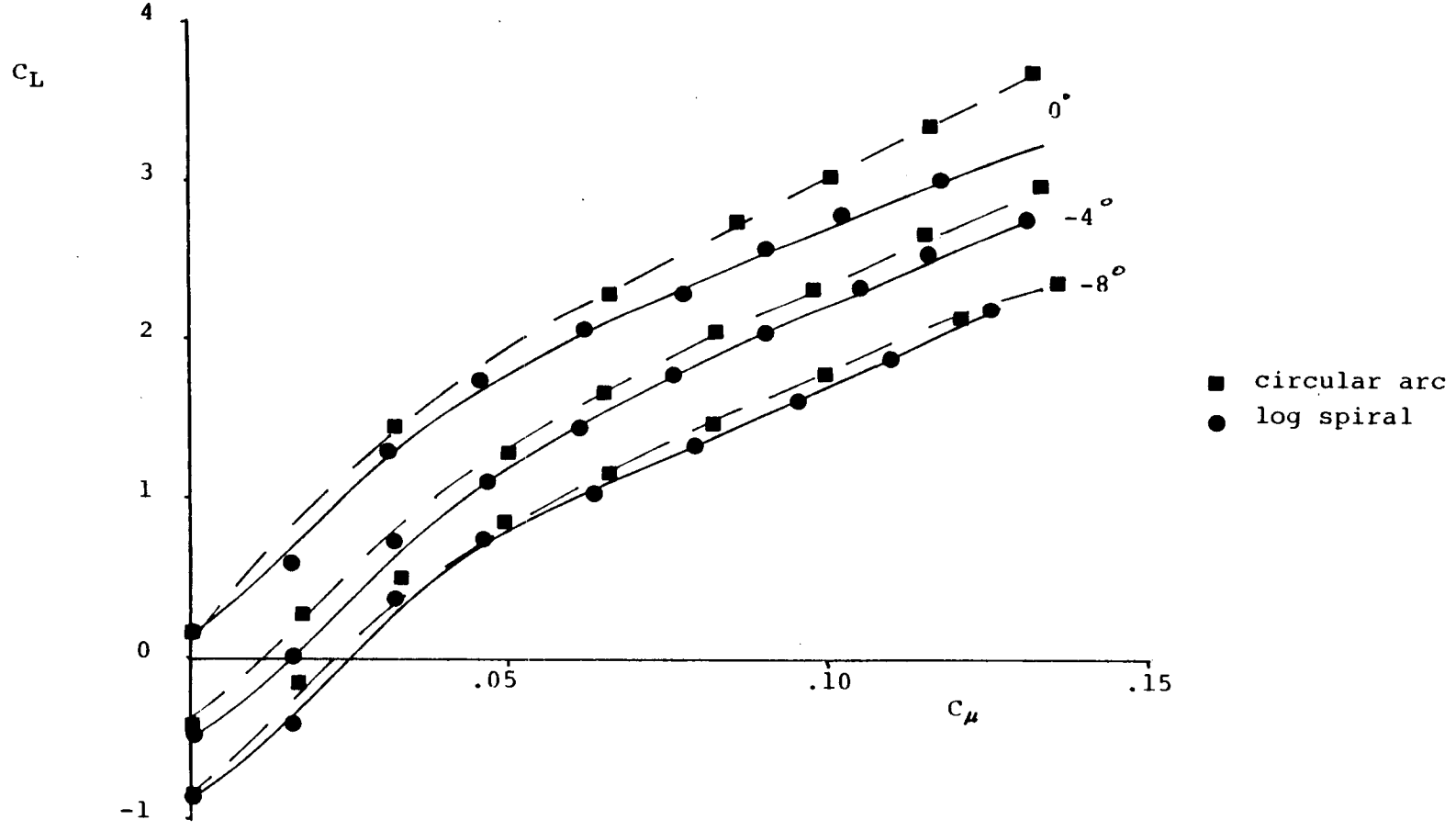

Fig. 17 Lift Coefficient vs. Momentum Coefficient: Trailing Edge Geometry Comparison (h/c = .0022).

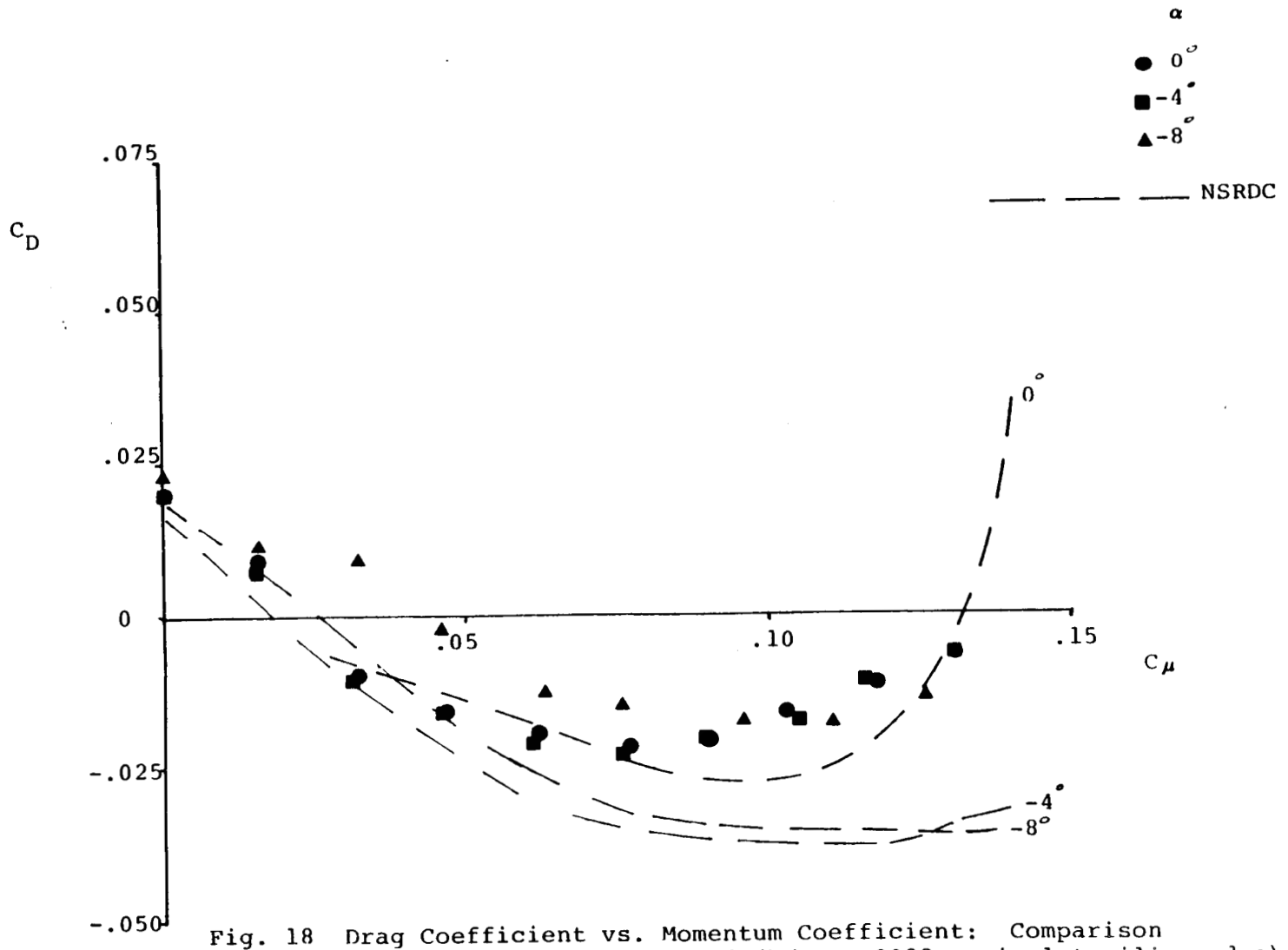

Fig. 18 Drag Coefficient vs. Momentum Coefficient: Comparison between NSRDC and Stanford (h/c = .0022, spiral trailing edge).

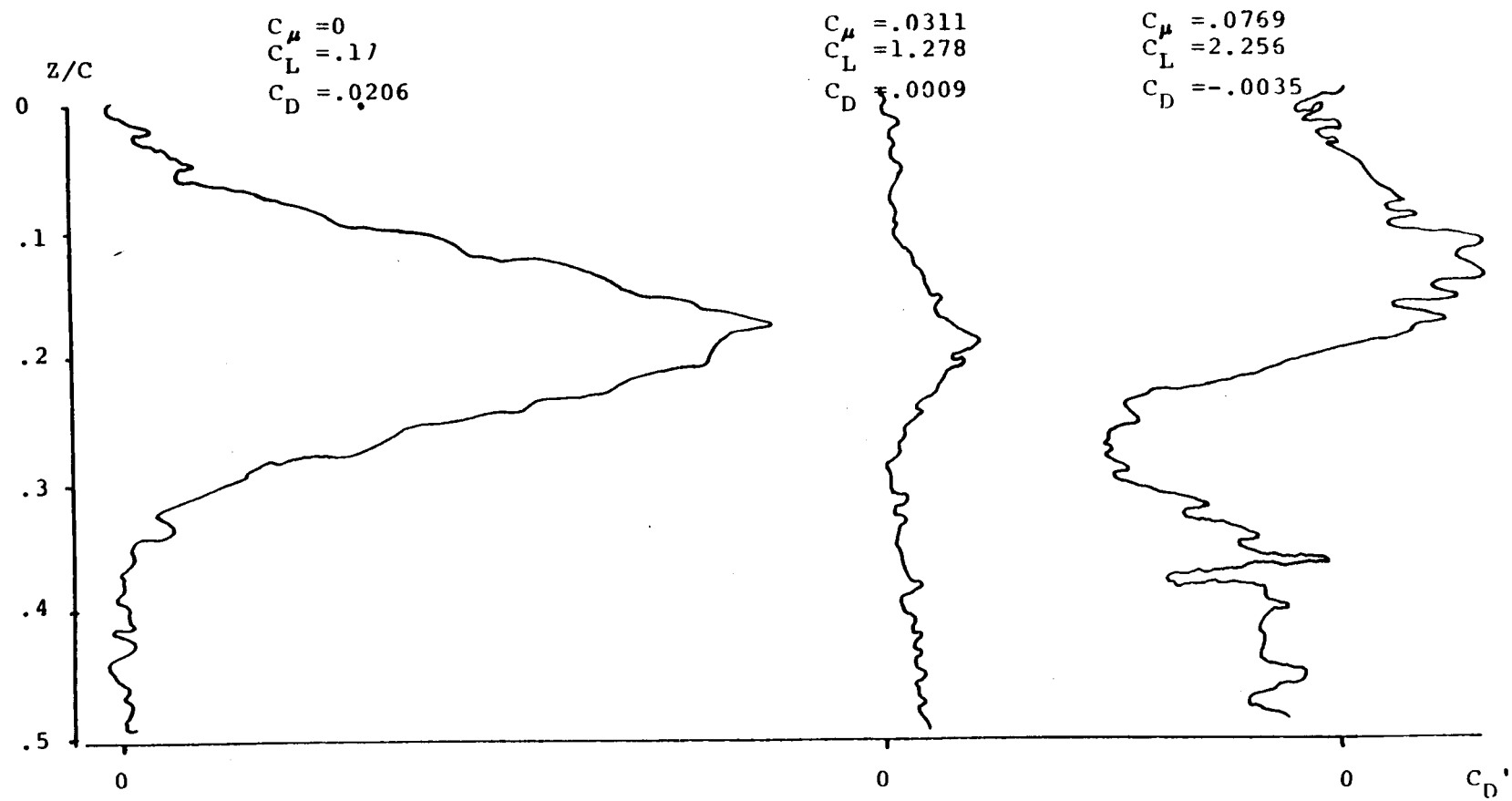

Fig. 19 Wake Profiles at One Chordlength Behind Model (0° incidence).
(increasing blowing ⟶)

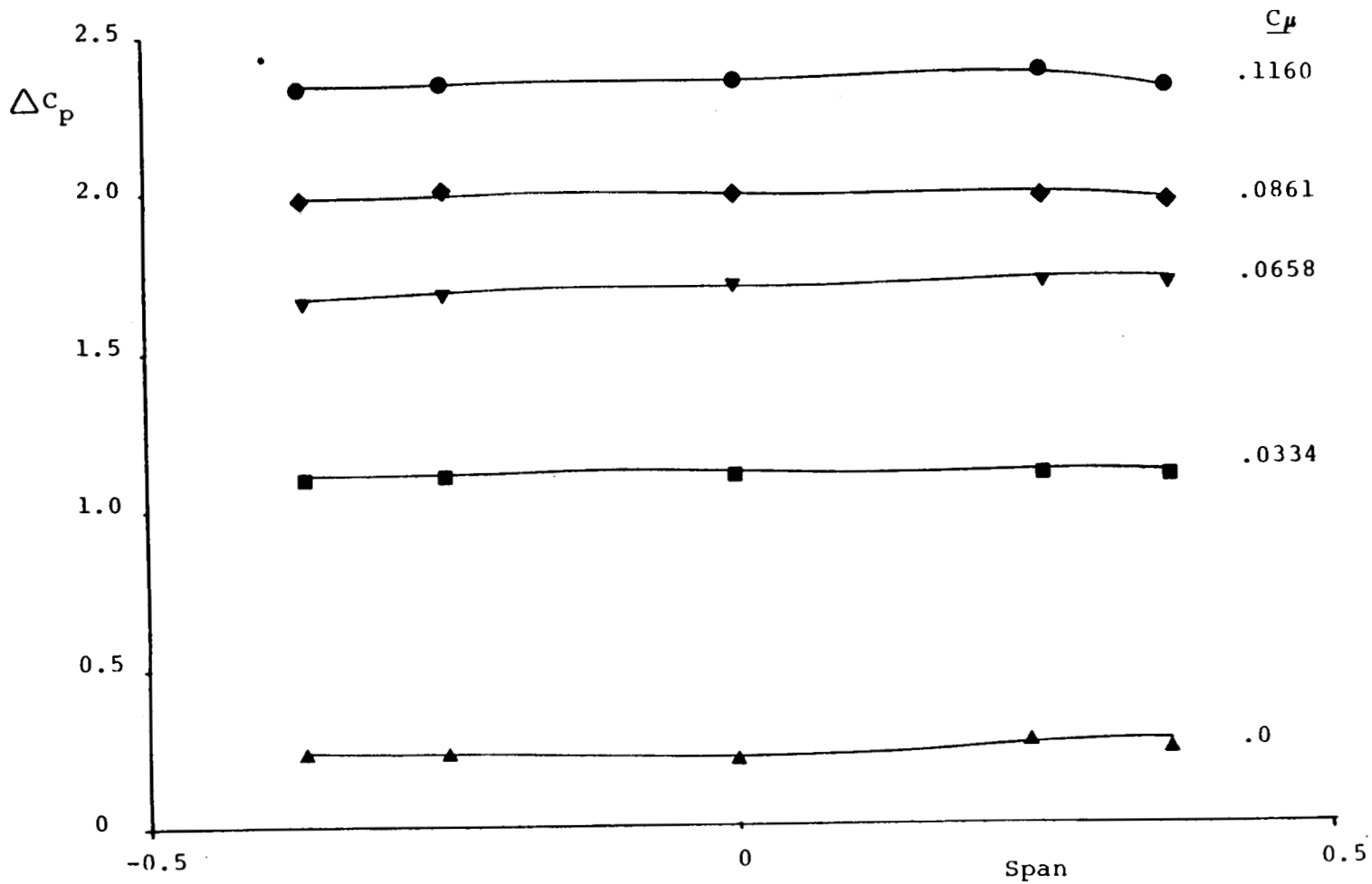

Fig. 20 Spanwise Lift Variation for Straight Slot (0° incidence).

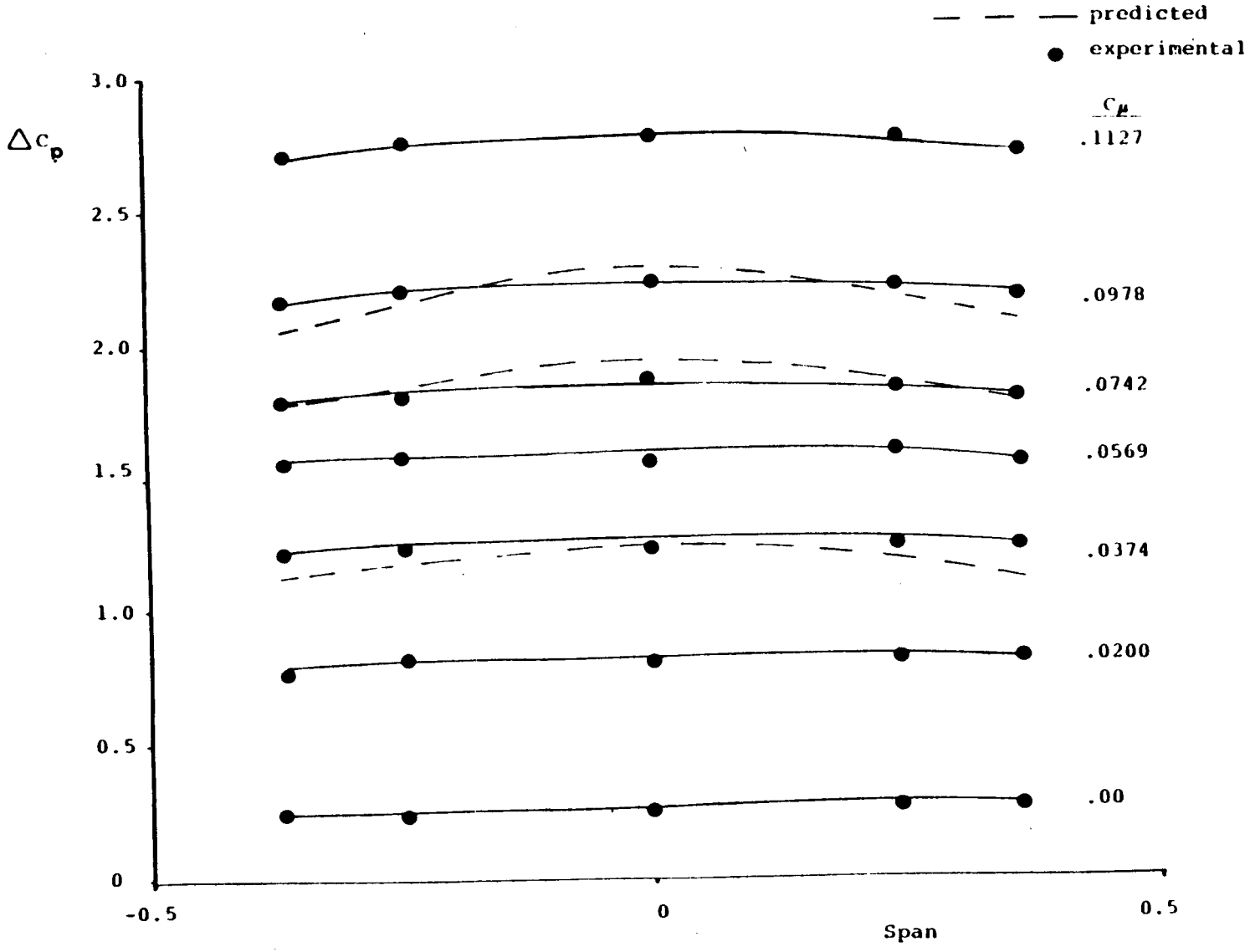

Fig. 21 Experimental vs. Predicted Spanwise Lift Variation with Slot Height Distribution (0 incidence).

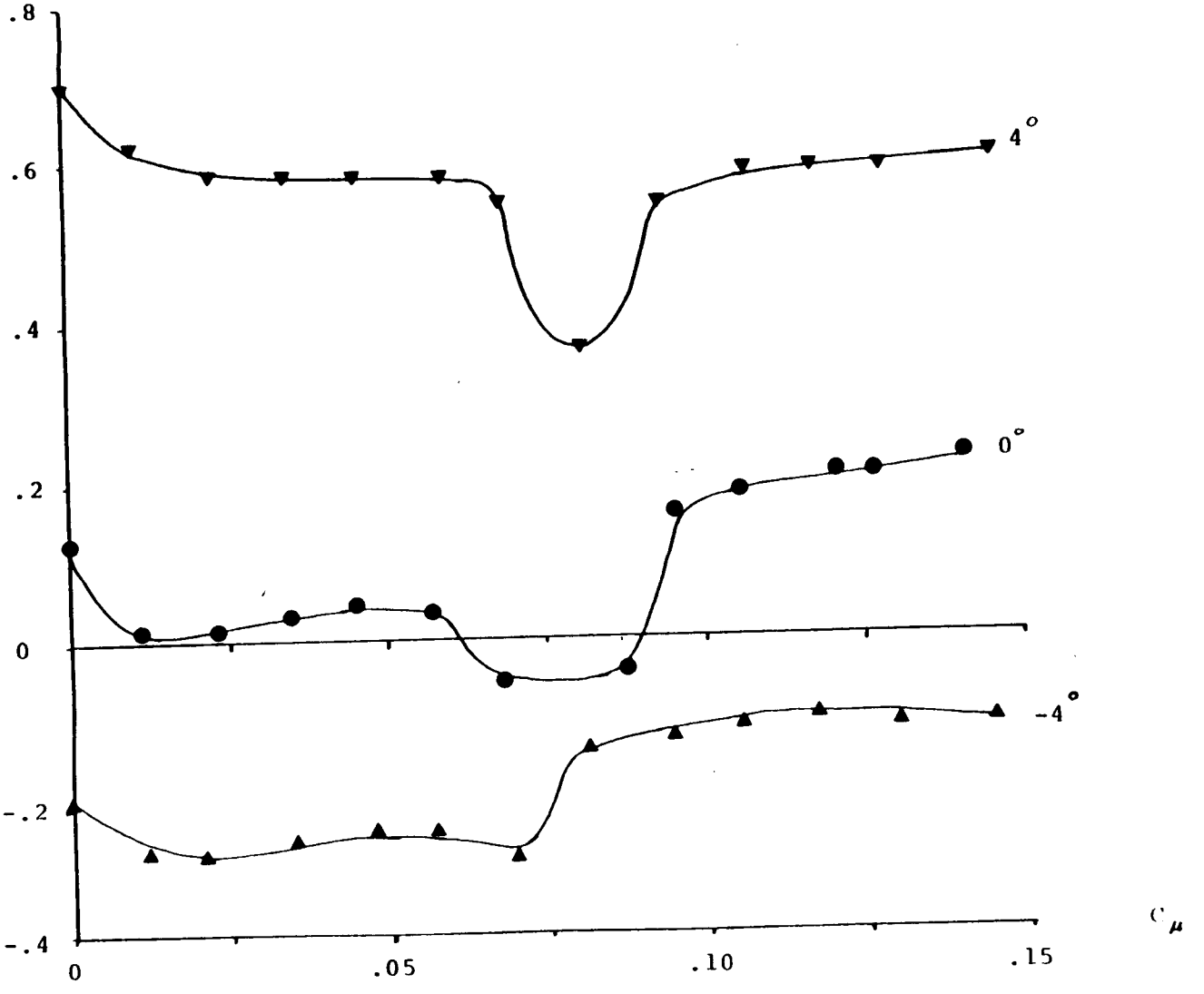

Fig. 22 Lift Coefficient vs. Leading Edge Blowing Momentum Coefficient (h/c=.0015).

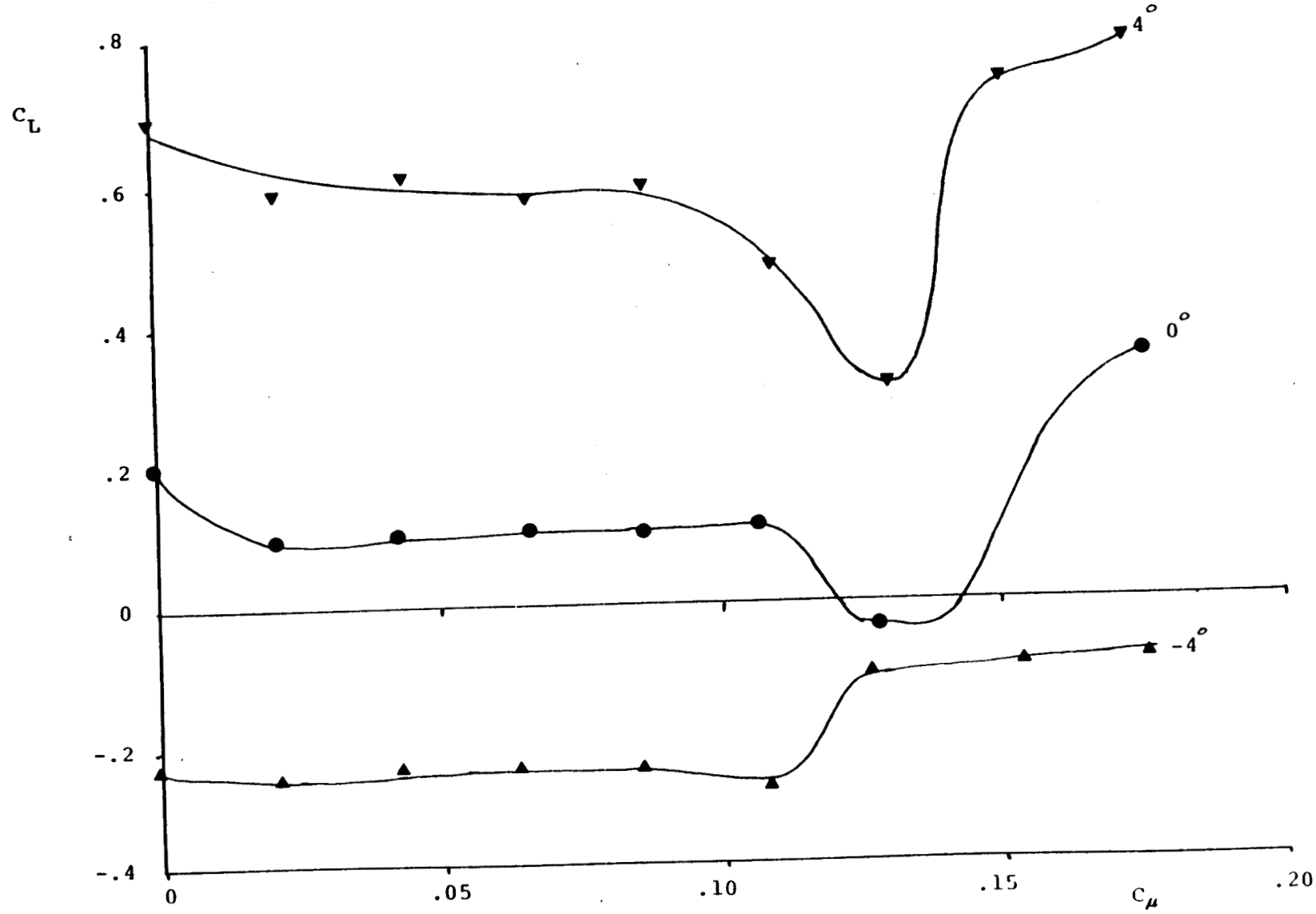

Fig. 23 Lift Coefficient vs. Leading Edge Blowing Momentum Coefficient (h/c=.003).

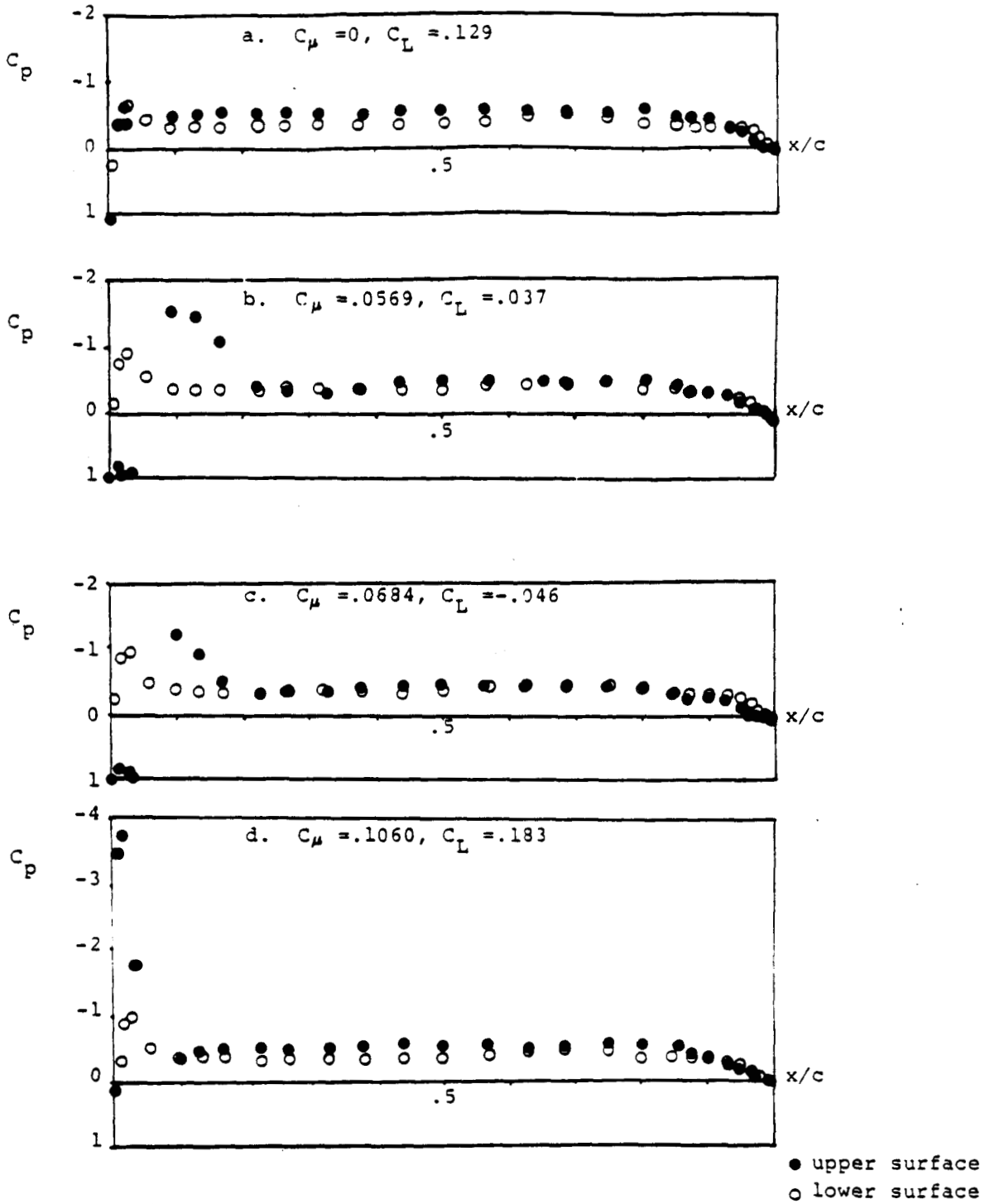

Fig. 24 Leading Edge Blowing Pressure Distributions (h/c = .0015).

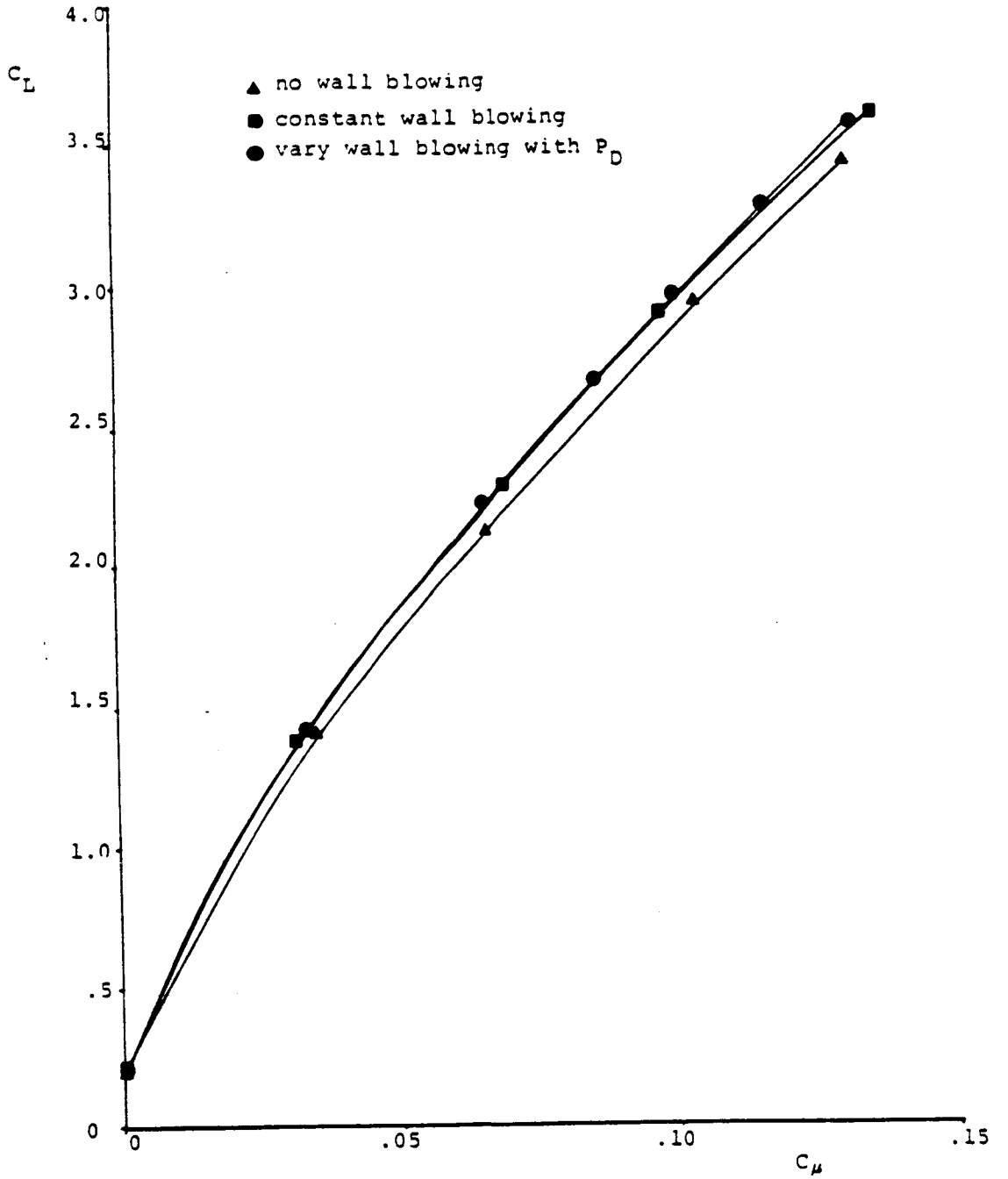

Fig. 25 Wall Blowing Effects on Lift Coefficient (h/c=.0022, 0° incidenc

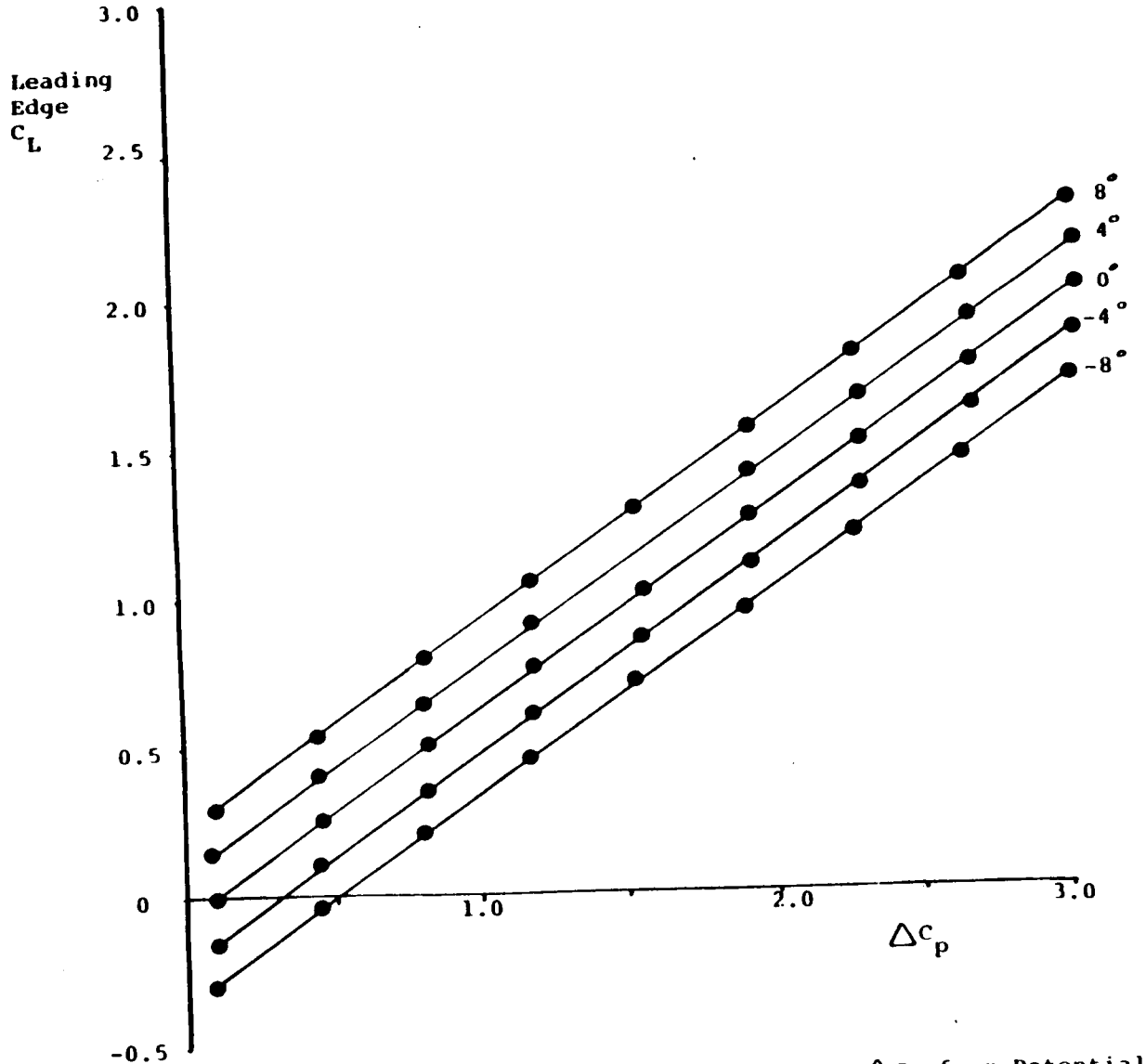

Fig. 26 Leading Edge Lift Coefficient vs. ΔC_p from Potential Flow.

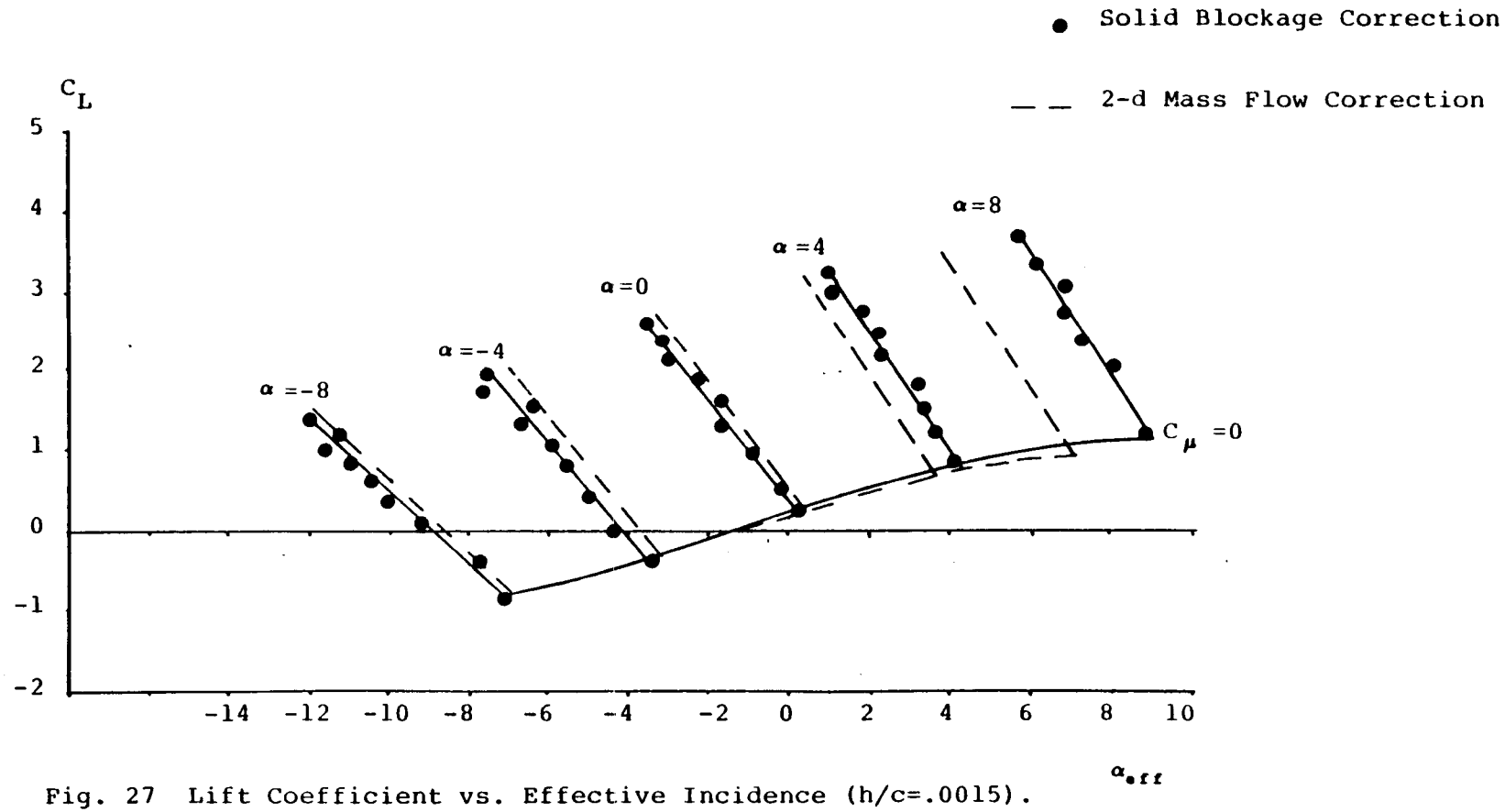

Fig. 27 Lift Coefficient vs. Effective Incidence (h/c=.0015).

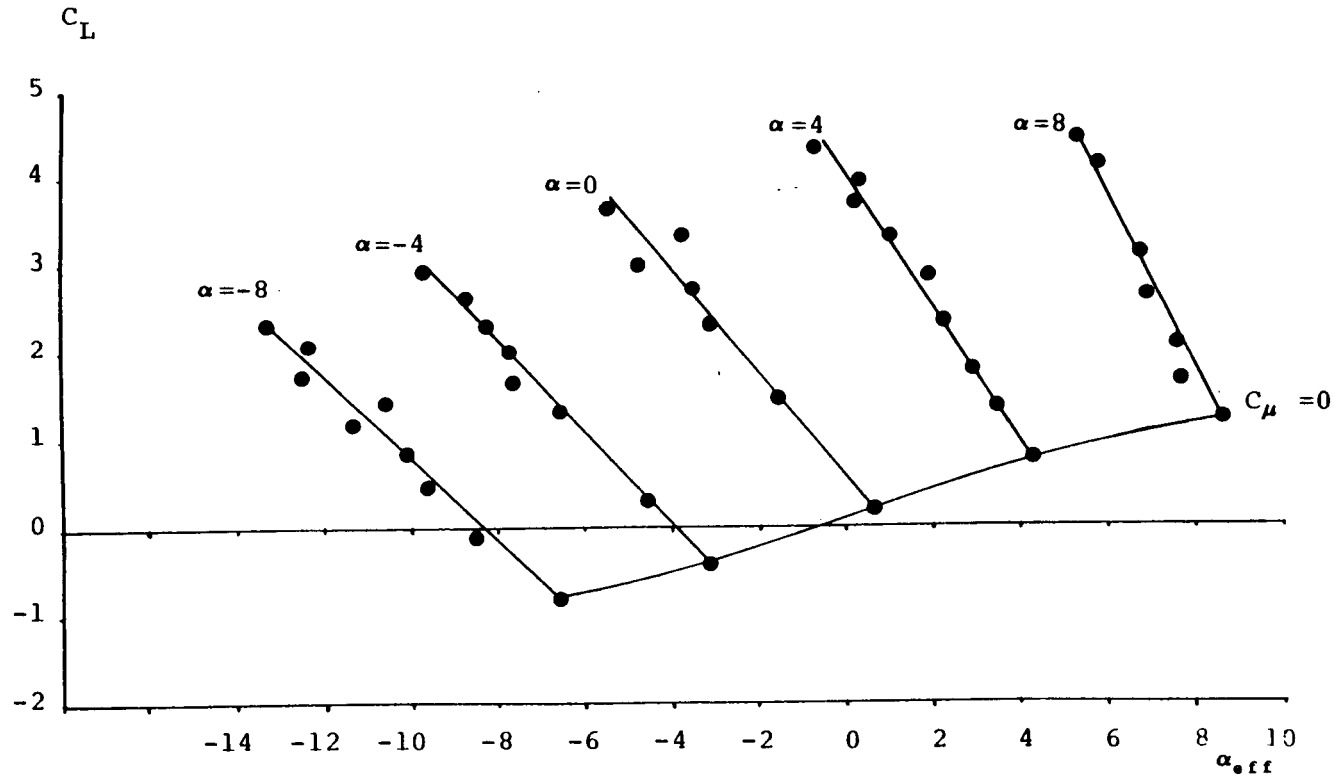

Fig. 28 Lift Coefficient vs. Effective Incidence (h/c = .0022).

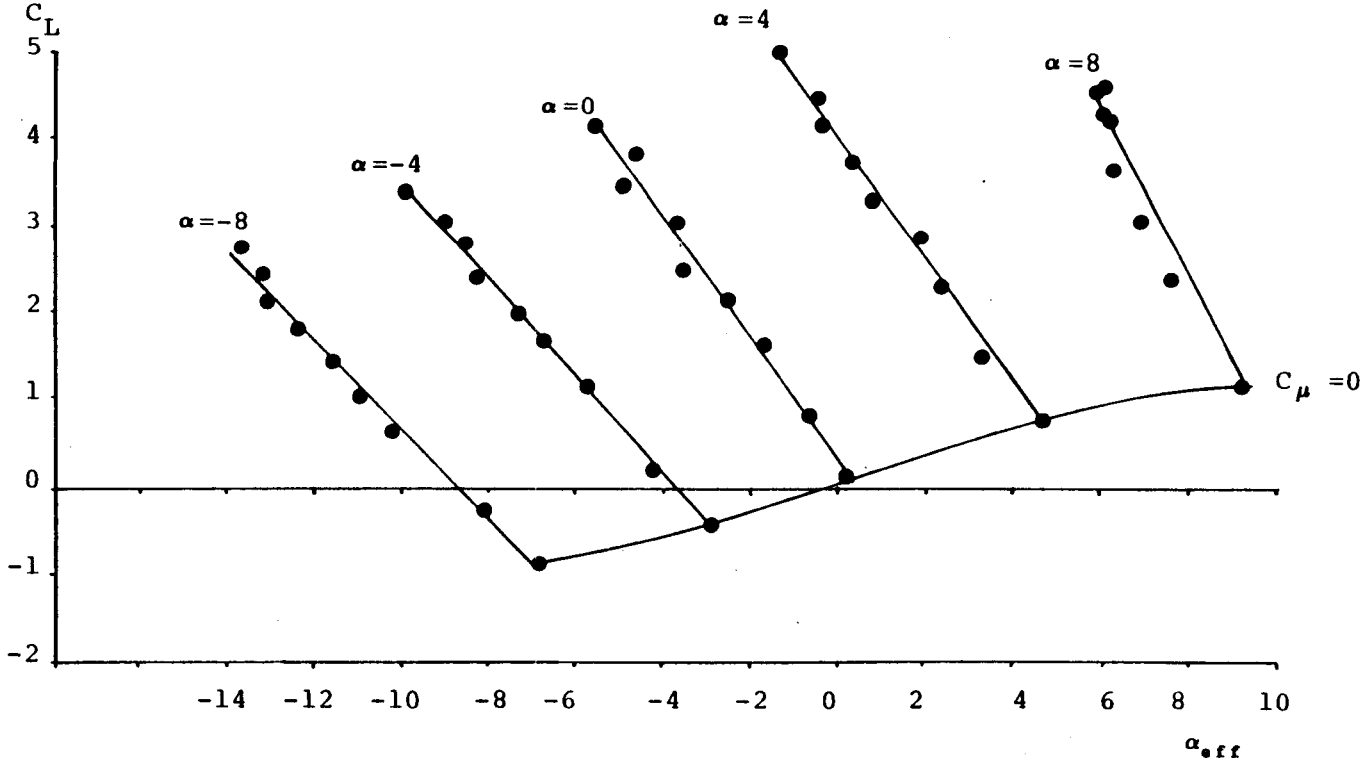

Fig. 29 Lift Coefficient vs. Effective Incidence (h/c=.003).

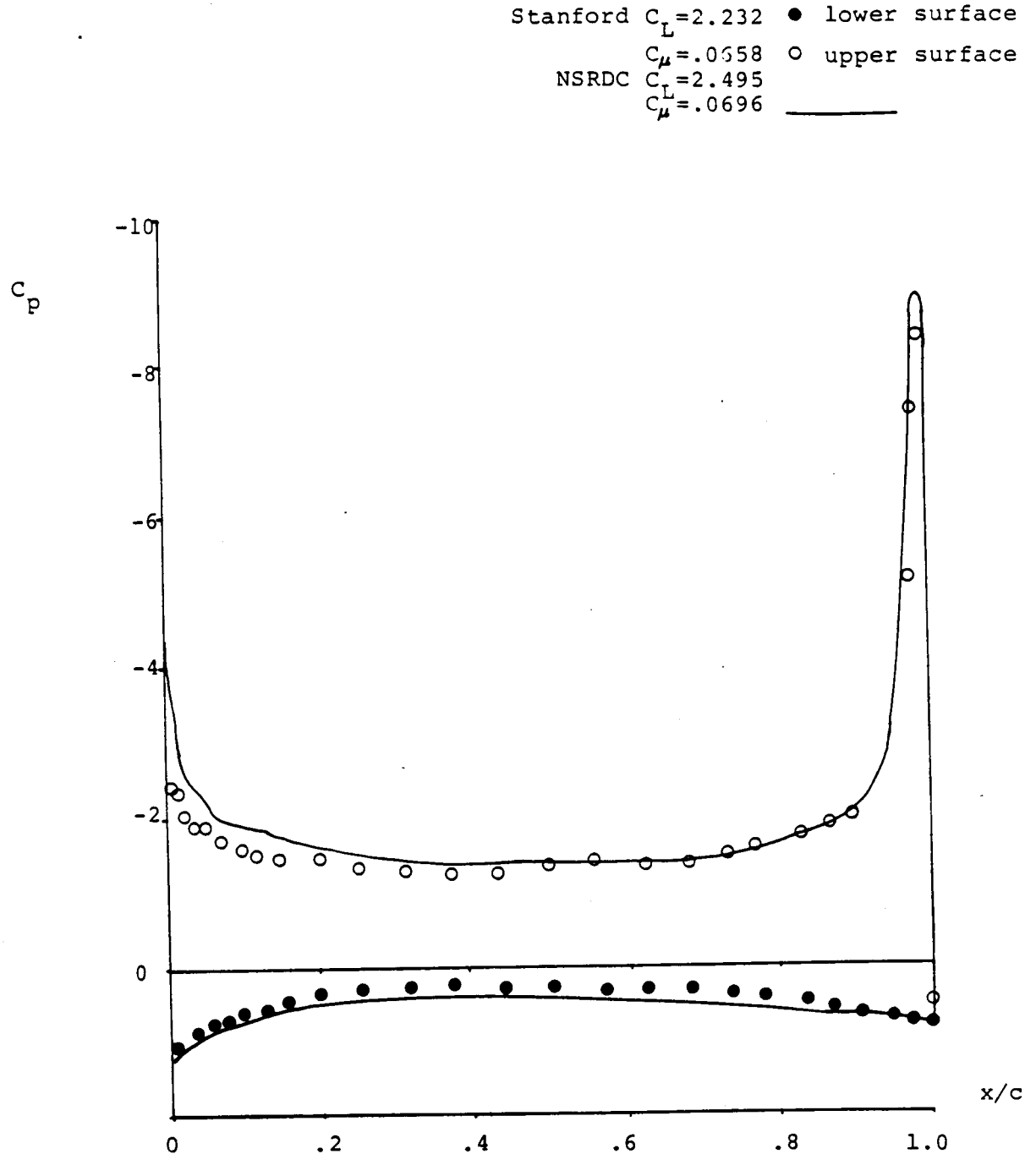

Fig. 30 Pressure Distribution Comparison Between NSRDC and Stanford (h/c=.0022).

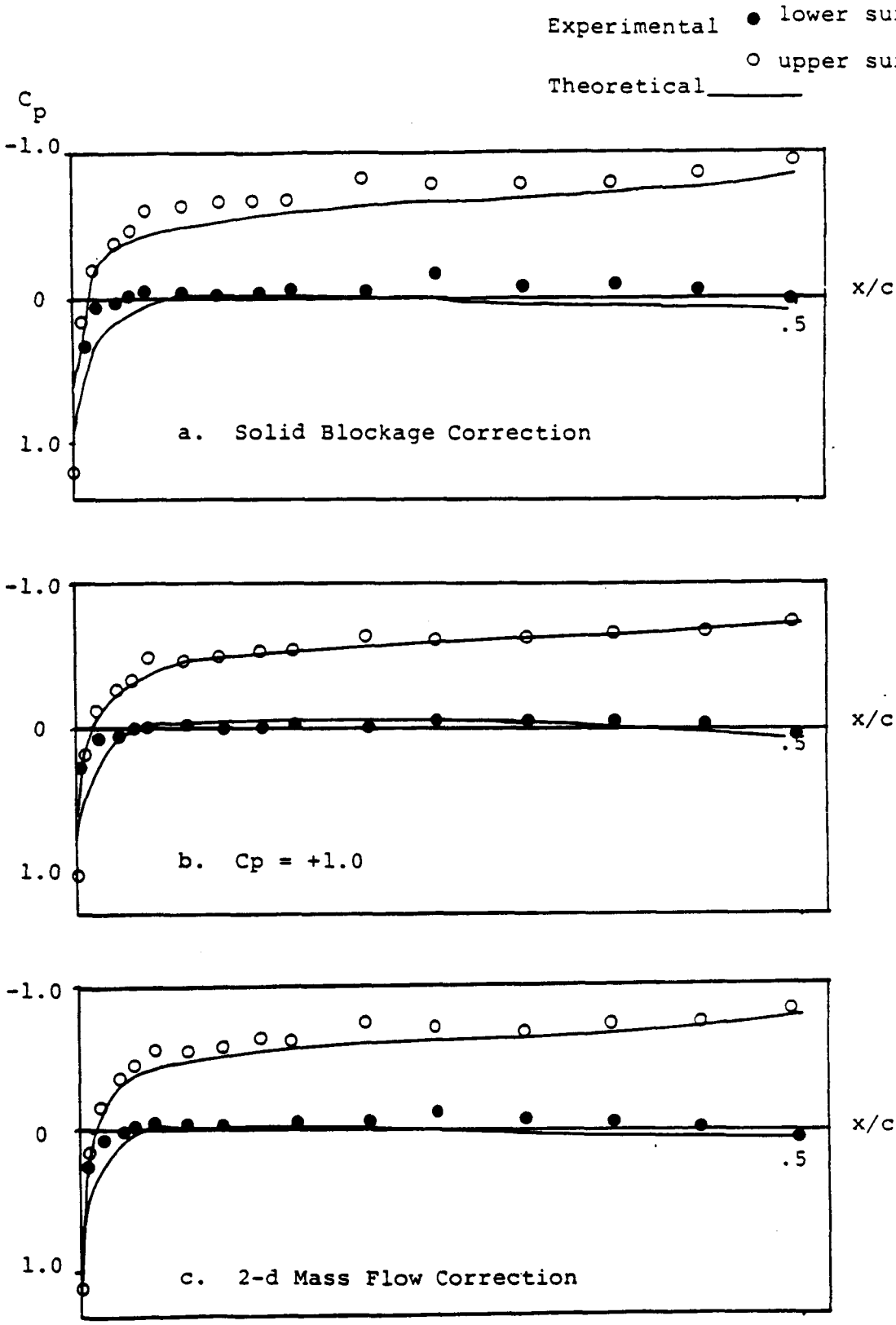

Fig. 31 Experimental vs. Theoretical Pressure Distributions ($\alpha = -4^\circ$, $C_\mu = .0492$).

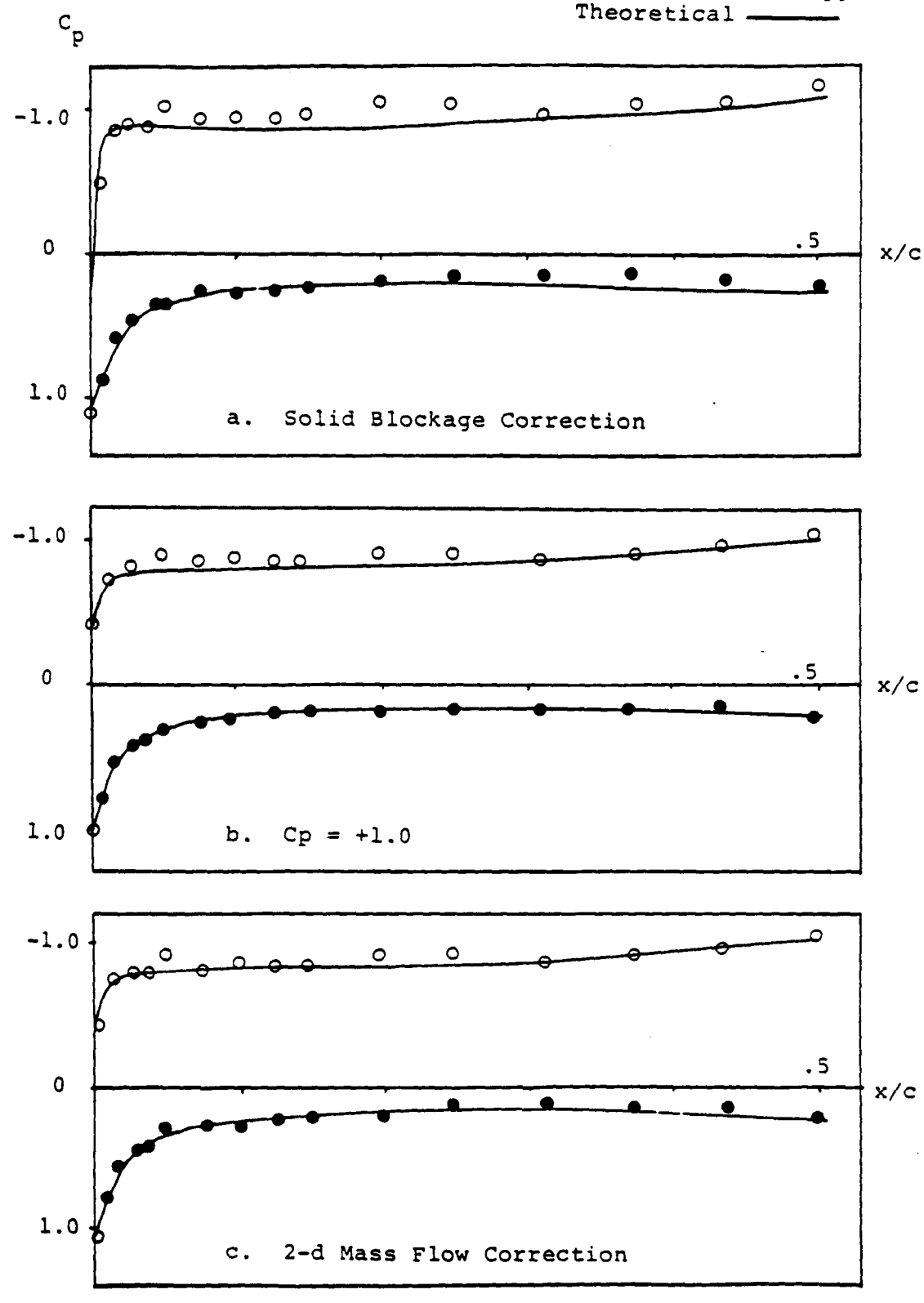

Fig. 32 Experimental vs. Theoretical Pressure Distributions ($\alpha = -4^\circ$, $C_\mu = .0927$).

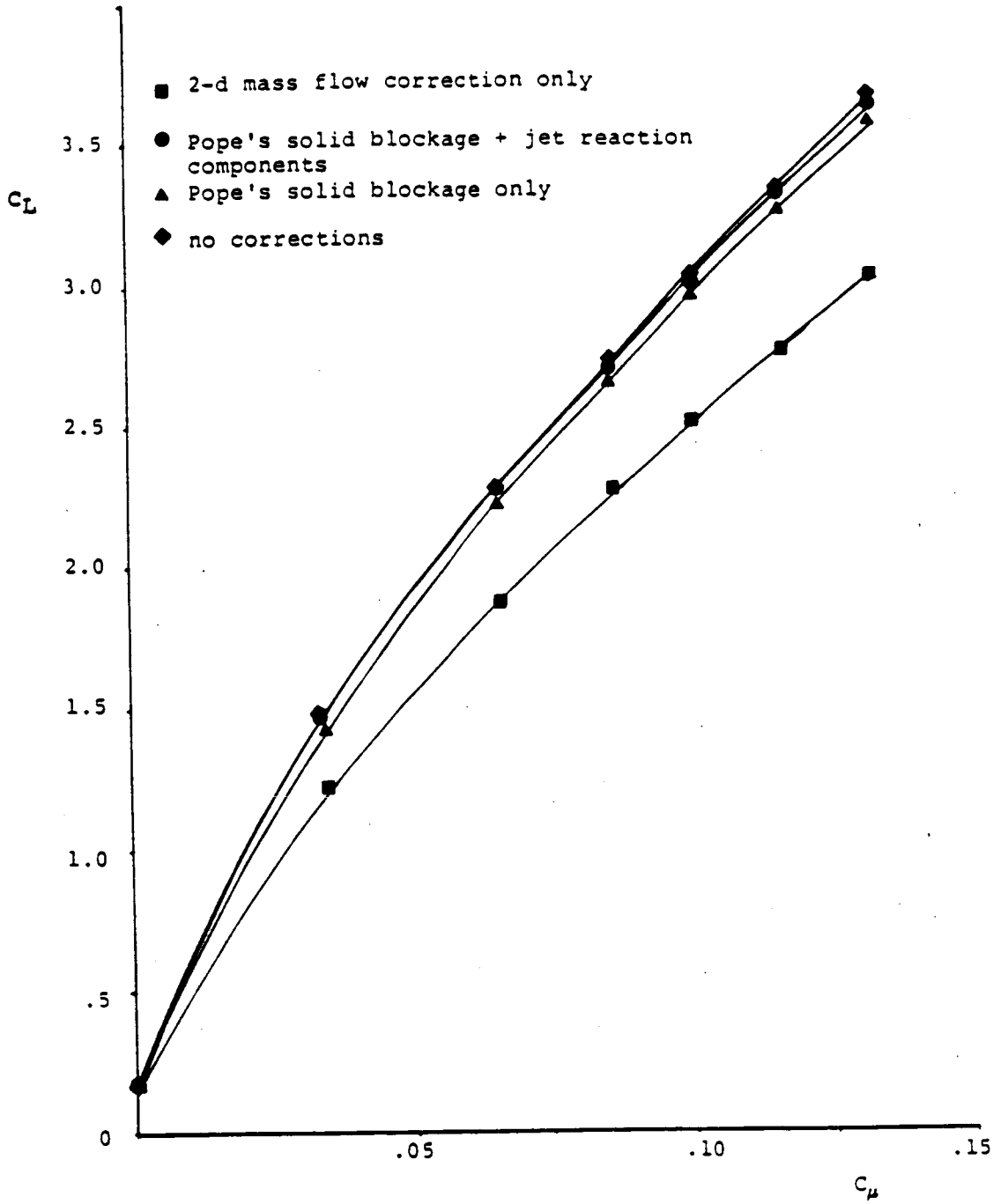

Fig. 33 The Effect of Solid Blockage Correction on Lift (h/c=.0022, 0° incidence).

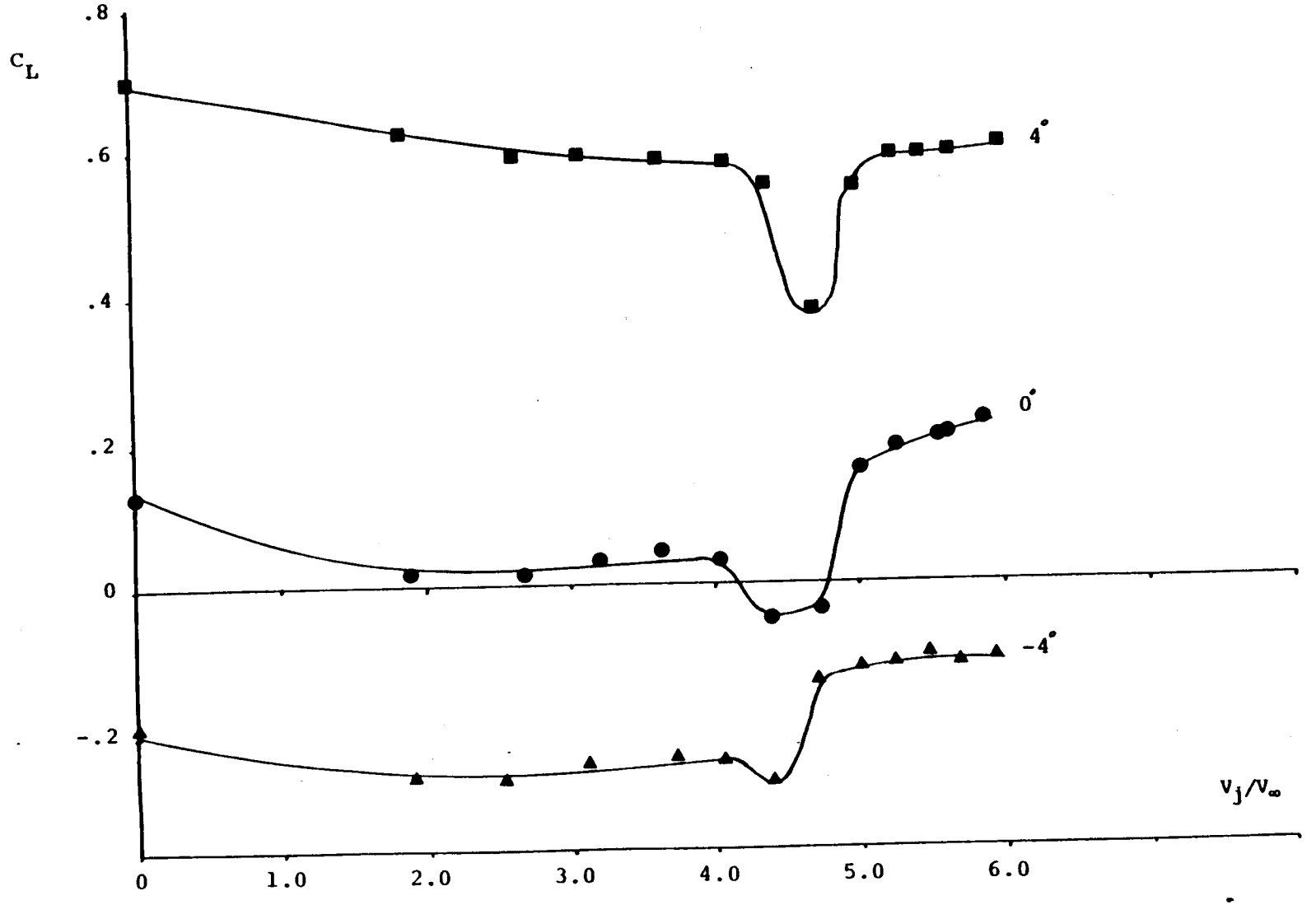

Fig. 34 Lift Coefficient vs. Leading Edge Blowing Jet Velocity Ratio (h/c=.0015).

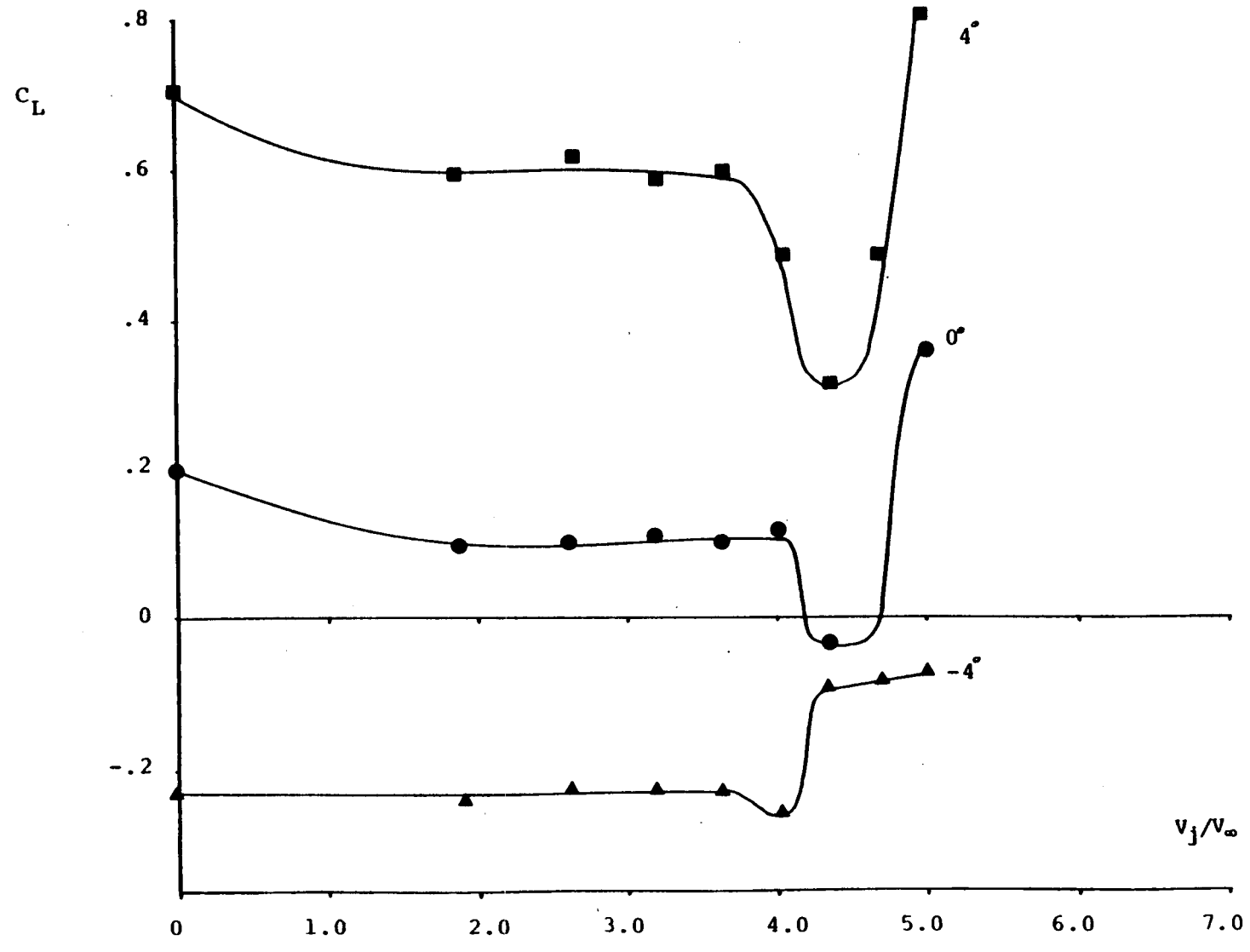

Fig. 35 Lift Coefficient vs. Leading Edge Blowing Jet Velocity Ratio (h/c=.003).

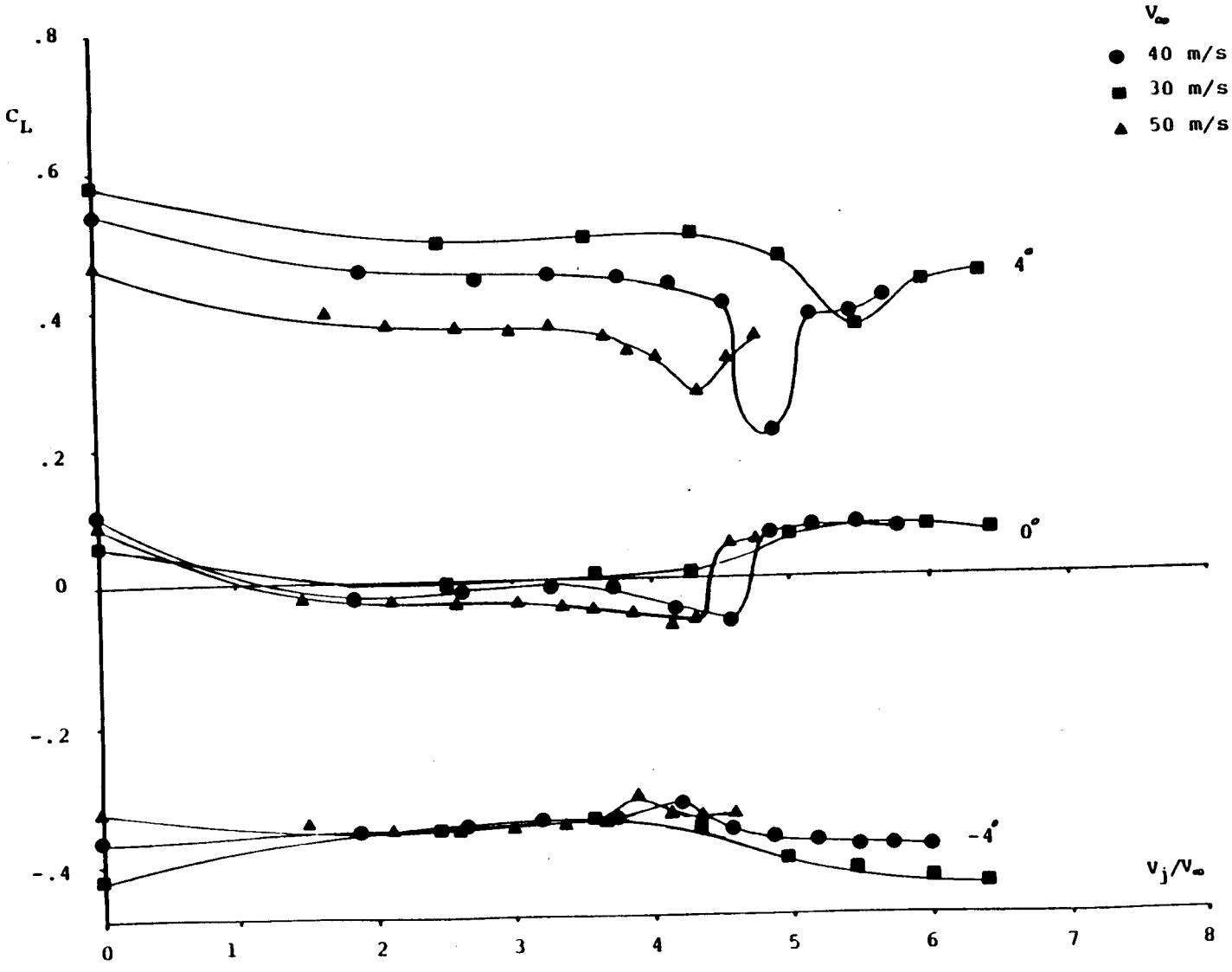

Fig. 36 Lift Coefficient Vs. Leading Edge Blowing Jet Velocity Ratio, for various free stream velocities (h/c = .0015).

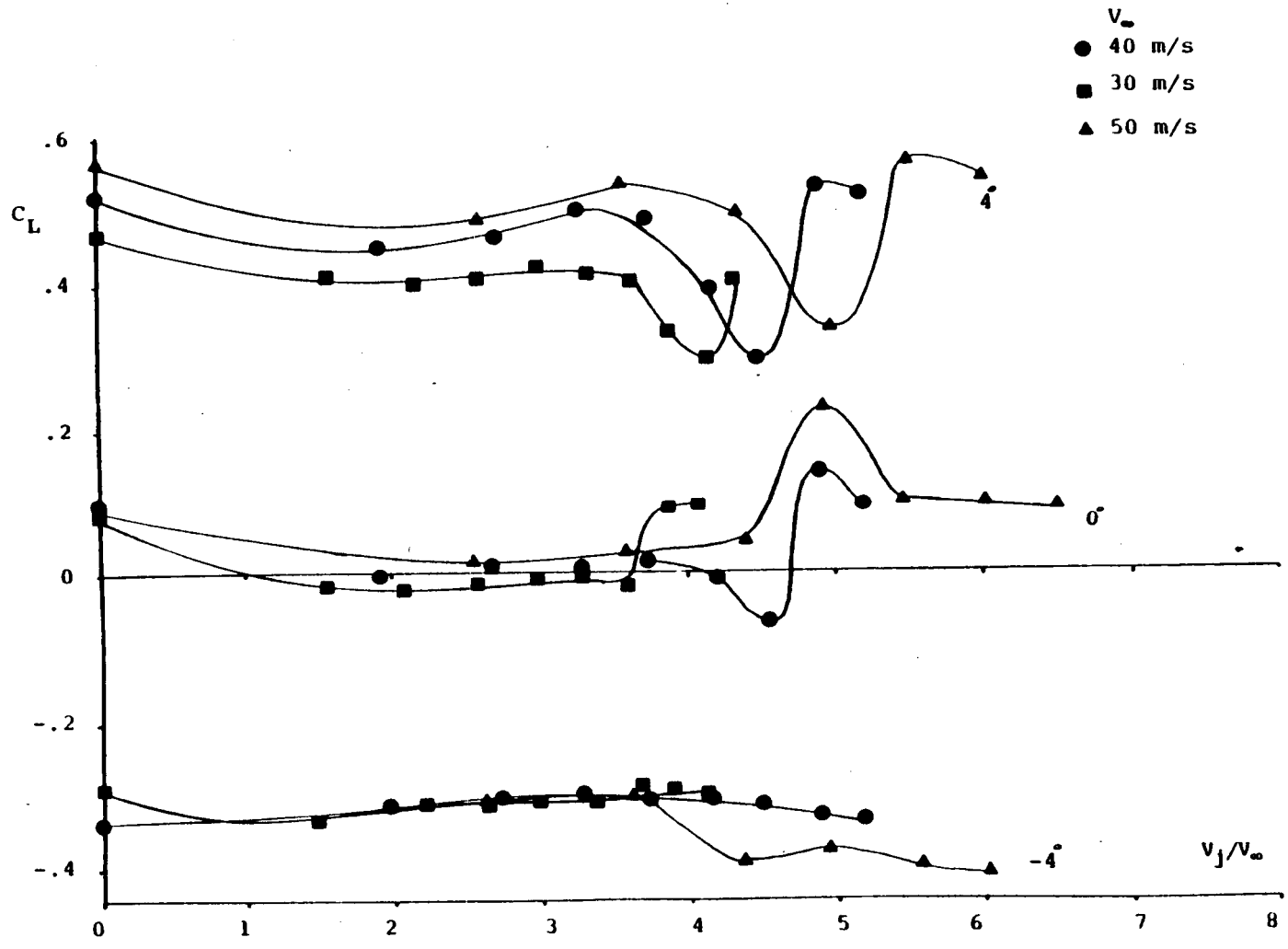

Fig. 37 Lift Coefficient vs. Leading Edge Blowing Jet Velocity Ratio, for various free stream velocities (h/c = .003).

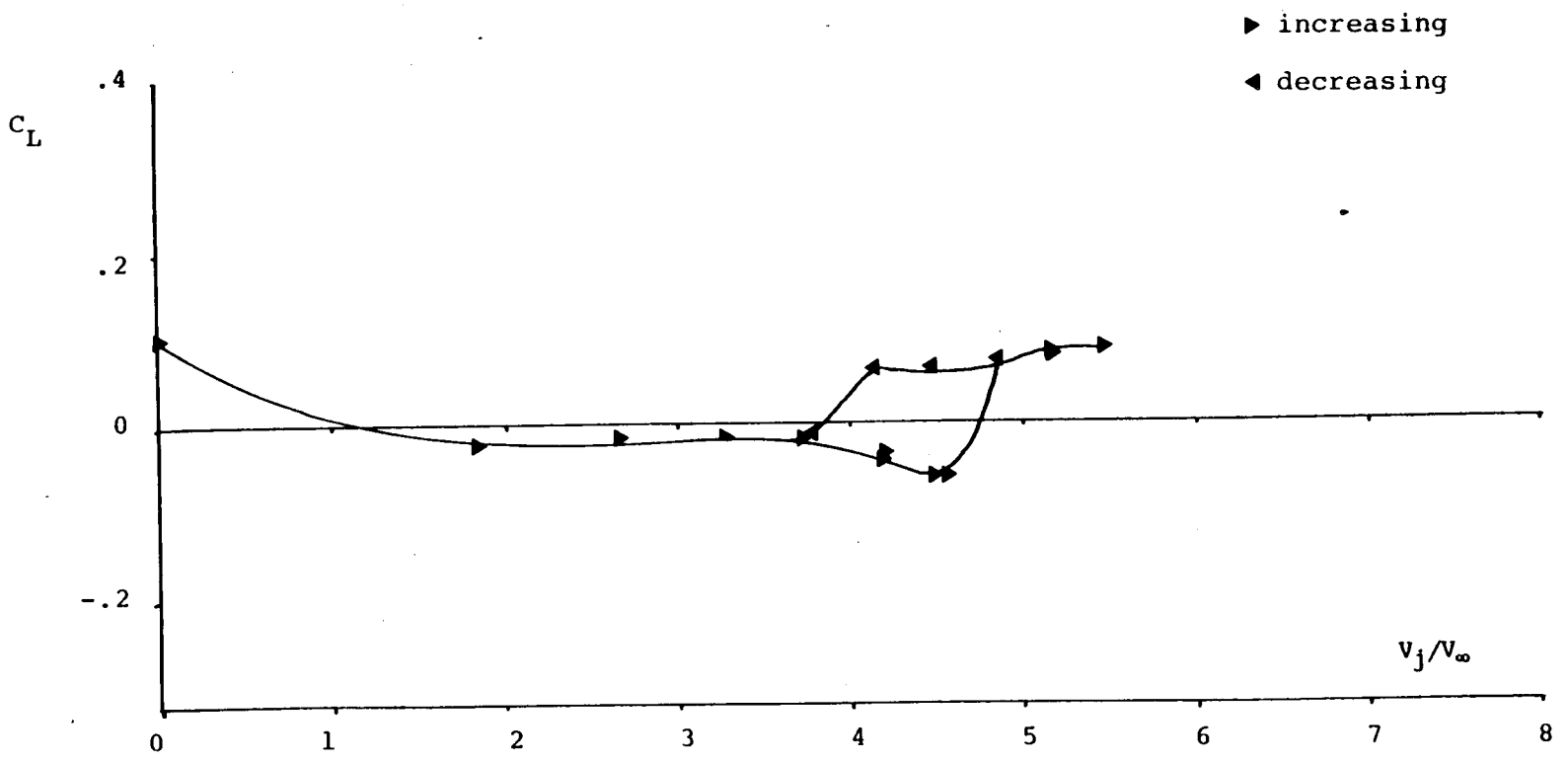

Fig. 38 Lift Coefficient vs. Leading Edge Blowing Jet Velocity Ratio: Hysteresis Effect (h/c = .0015, 0° incidence, V_∞ = 40 m/s).